The Plant Cell, Vol. 18, 3576–3593, December 2006, www.plantcell.org

The Essential Nature of Sphingolipids in Plants as Revealed by the Functional Identification and Characterization of the *Arabidopsis* LCB1 Subunit of Serine Palmitoyltransferase [W]

Ming Chen,[a] Gongshe Han,[b] Charles R. Dietrich,[c] Teresa M. Dunn,[b] and Edgar B. Cahoon[c,1]

[a] Donald Danforth Plant Science Center, St. Louis, Missouri 63132
[b] Department of Biochemistry and Molecular Biology, Uniformed Services University of the Health Sciences, Bethesda, Maryland 20814
[c] U.S. Department of Agriculture–Agricultural Research Service, Plant Genetics Research Unit, Donald Danforth Plant Science Center, St. Louis, Missouri 63132

Serine palmitoyltransferase (SPT) catalyzes the first step of sphingolipid biosynthesis. In yeast and mammalian cells, SPT is a heterodimer that consists of LCB1 and LCB2 subunits, which together form the active site of this enzyme. We show that the predicted gene for *Arabidopsis thaliana* LCB1 encodes a genuine subunit of SPT that rescues the sphingolipid long-chain base auxotrophy of *Saccharomyces cerevisiae* SPT mutants when coexpressed with *Arabidopsis* LCB2. In addition, homozygous T-DNA insertion mutants for At *LCB1* were not recoverable, but viability was restored by complementation with the wild-type At *LCB1* gene. Furthermore, partial RNA interference (RNAi) suppression of At *LCB1* expression was accompanied by a marked reduction in plant size that resulted primarily from reduced cell expansion. Sphingolipid content on a weight basis was not changed significantly in the RNAi suppression plants, suggesting that plants compensate for the downregulation of sphingolipid synthesis by reduced growth. At *LCB1* RNAi suppression plants also displayed altered leaf morphology and increases in relative amounts of saturated sphingolipid long-chain bases. These results demonstrate that plant SPT is a heteromeric enzyme and that sphingolipids are essential components of plant cells and contribute to growth and development.

INTRODUCTION

Sphingolipids are major components of the plasma membrane and tonoplast of plant cells (Yoshida and Uemura, 1986; Lynch and Steponkus, 1987; Sperling et al., 2005). In addition to serving a structural role in membranes, sphingolipids, along with sterols, are enriched in detergent-resistant membranes (or lipid rafts) prepared from the plasma membrane of plant cells (Mongrand et al., 2004; Borner et al., 2005). Lipid rafts have been linked to the sorting and trafficking of specific plasma membrane proteins, including ATPases, arabinogalactan proteins, and glycosylphosphatidylinositol-anchored proteins, which are involved in a range of cellular activities, including cell wall synthesis and degradation and possibly signaling (Borner et al., 2005). In addition, sphingolipid-derived molecules have been shown to function as signaling molecules and to initiate programmed cell death in plants. The sphingolipid metabolites sphingosine-1-phosphate and, more recently, phytosphingosine-1-phosphate, for example, have been shown to mediate abscisic acid–dependent guard cell closure by transduction through the sole prototypical G-protein α-subunit GPA1 (Ng et al., 2001; Coursol et al., 2003, 2005). Disruption of a sphingolipid ceramide kinase gene has also been identified as the basis for the enhanced rate of apoptosis in the *Arabidopsis thaliana accelerated cell death5* mutant, suggesting that levels of the ceramide component of sphingolipids regulate programmed cell death in plants (Liang et al., 2003). Similarly, inhibition of ceramide synthase by the fungal toxins fumonisin and AAL toxin has also been shown to promote apoptosis (Wang et al., 1996; Spassieva et al., 2002).

Sphingolipids in plants are composed of a ceramide backbone that consists of a C_{18} long-chain base bound to a fatty acid via an amide linkage. The long-chain bases and fatty acids can contain differing numbers of hydroxyl groups and degrees of unsaturation, and the fatty acid components typically contain 16 to 26 carbon atoms (Lynch and Dunn, 2003). The ceramide is substituted at its terminal hydroxyl group with polar residues, including carbohydrate, phosphoinositol, and phosphocholine moieties, to form complex sphingolipids. The major complex sphingolipids identified to date in plants are monoglucosylceramides, also called glucocerebrosides, which contain a glucose head group, and the more polar inositol phosphate–based sphingolipids, which are collectively referred to as inositolphosphoceramides (Carter et al., 1961; Kaul and Lester, 1978).

Despite the important roles that sphingolipids play in membranes and in intracellular processes such as signal transduction and programmed cell death, little is known about the regulation of their biosynthesis in plants. In yeast and mammalian cells, regulation of sphingolipid synthesis is believed to occur largely at the initial step of the pathway. This reaction involves the condensation of palmitoyl-CoA and Ser to form 3-ketosphinganine, the precursor of long-chain bases, and is catalyzed by serine

[1] To whom correspondence should be addressed. E-mail ecahoon@danforthcenter.org; fax 314-587-1391.
The author responsible for distribution of materials integral to the findings presented in this article in accordance with the policy described in the Instructions for Authors (www.plantcell.org) is: Edgar B. Cahoon (ecahoon@danforthcenter.org).
[W] Online version contains Web-only data.
www.plantcell.org/cgi/doi/10.1105/tpc.105.040774

palmitoyltransferase (SPT) (Hanada, 2003) (Figure 1). The activity of this enzyme requires the cofactor pyridoxal 5′-phosphate, which is bound through a Schiff's base to an active site Lys. Regulation of SPT in mammals has been shown to occur at both the transcriptional and posttranscriptional levels (Hanada, 2003). Sphingolipids occur primarily in eukaryotes, but they are also found in several bacterial genera, most notably *Sphingomonas* species, in which they function as cell wall components (Ikushiro et al., 2001). The bacterial and eukaryotic SPTs display distinct differences in their intracellular localization and structure. SPT of *Sphingomonas* species is a soluble homodimer (Ikushiro et al., 2001). By contrast, all known eukaryotic SPTs are membrane-associated heterodimers that are composed of subunits encoded by the *LCB1* and *LCB2* genes (Hanada, 2003) (Figure 1). The LCB1 and LCB2 subunits from *Saccharomyces cerevisiae* and mammals have been studied most extensively. The LCB2 subunit from these organisms contains the active site Lys that binds the pyridoxal phosphate cofactor. This residue is absent from the LCB1 subunit. Although LCB1 lacks a catalytic Lys residue, data from modeling and mutational studies indicate that the active site of SPT lies at the interface of the heterodimeric enzyme and that residues from both subunits are involved in catalysis (Gable et al., 2002). In addition, LCB1 stabilizes LCB2, as the lack of LCB1 in *S. cerevisiae* (Gable et al., 2000) and in Chinese hamster ovary (CHO) cells (Yasuda et al., 2003) results in large reductions in the amount of LCB2 protein. Furthermore, loss-of-function mutations in either the *LCB1* or the *LCB2* genes of yeast (Buede et al., 1991; Nagiec et al., 1994; Zhao et al., 1994), mammalian cells (Hanada et al., 1992), and *Drosophila* (Adachi-Yamada et al., 1999) are lethal. Because SPT is the initial enzyme in the sphingolipid biosynthetic pathway, these results demonstrate that sphingolipids are essential for the viability of yeast, mammalian, and insect cells.

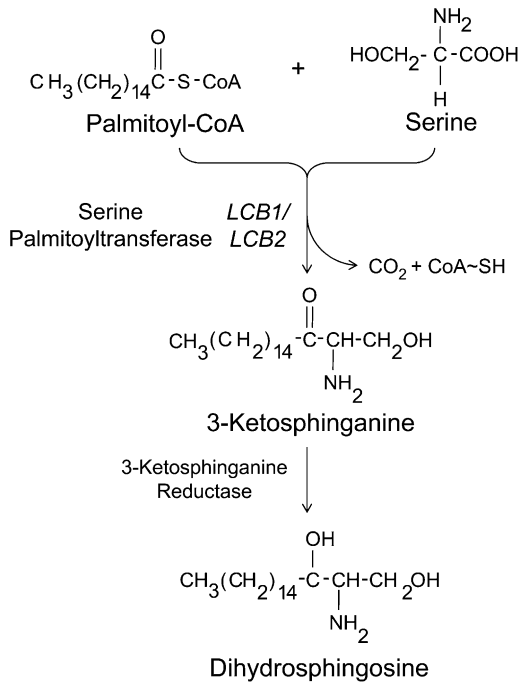

Figure 1. Biosynthesis of Sphingolipid Long-Chain Bases.

The first step in the synthesis of sphingolipid long-chain bases is the condensation of Ser and palmitoyl-CoA, which is catalyzed by SPT. Eukaryotic forms of SPT are composed of subunits designated LCB1 and LCB2. The 3-ketosphinganine product of SPT is reduced by 3-ketosphinganine reductase to form dihydrosphingosine (d18:0), the simplest long-chain base. Other long-chain bases are formed by further hydroxylation and desaturation of dihydrosphingosine.

Although it can be presumed that the plant SPT is also a heterodimer of LCB1 and LCB2 subunits, this structural composition has not been demonstrated previously. A cDNA for an *Arabidopsis* LCB2-related polypeptide has been identified and characterized (Tamura et al., 2001). Like other eukaryotic LCB2 polypeptides, the predicted *Arabidopsis* LCB2 (At5g23670, designated here as At LCB2) contains a pyridoxal phosphate binding motif, which includes the conserved Lys residue. Expression of At LCB2 in an *S. cerevisiae lcb2Δ* disruption mutant, however, did not result in sufficient SPT activity to complement the long-chain base auxotrophy of these cells (Tamura et al., 2001). This observation suggests that, like its counterparts from yeast and mammals, the *Arabidopsis* SPT is a heteromeric enzyme.

Arabidopsis contains a gene (At4g36480) that encodes a polypeptide with 31% identity to the *S. cerevisiae* LCB1. In this report, we demonstrate that this gene encodes a functional LCB1 subunit of SPT (designated At LCB1). As shown here, coexpression of the gene for At LCB1 with the gene for At LCB2 yields an active SPT that is able to rescue *S. cerevisiae lcb1Δ* and *lcb2Δ* single and double knockout mutants. We also show that sphingolipids are essential in *Arabidopsis* and that nonlethal reduction of At *LCB1* expression results in profound alterations in the growth and development of *Arabidopsis* and in the long-chain base composition of complex sphingolipids.

RESULTS

Arabidopsis Contains a Homolog of the Yeast and Mammalian LCB1 Subunit of SPT

SPT from all eukaryotes examined to date is an LCB1/LCB2 heterodimer (Hanada, 2003) (Figure 1). An LCB2 subunit (At LCB2) of the *Arabidopsis* SPT has been characterized previously (Tamura et al., 2001), but the LCB1 subunit has yet to be functionally identified. Homology searches of the *Arabidopsis* genome revealed a gene (At4g36840, At *LCB1*) encoding a polypeptide of the α-oxoamine synthase subfamily of pyridoxal phosphate–dependent enzymes with 31% identity to the *S. cerevisiae* and 41% identity to the *Homo sapiens* LCB1 polypeptides. At LCB1 is more distantly related to LCB2s (<25% identity), including At LCB2, as well as to other α-oxoamine synthases, such as the soluble bacterial SPT and 8-amino-7-oxononanonate synthase (AONS). At *LCB1* is a single-copy gene in *Arabidopsis*, but at least two copies of *LCB1*-like genes occur in the rice (*Oryza sativa*) genome, with map positions on chromosomes 2 and 10 (Figure 2A). Similar to the distinctive feature of all previously characterized LCB1 polypeptides (Gable et al., 2002), At LCB1 lacks an active site Lys, which is typically found in α-oxoamine

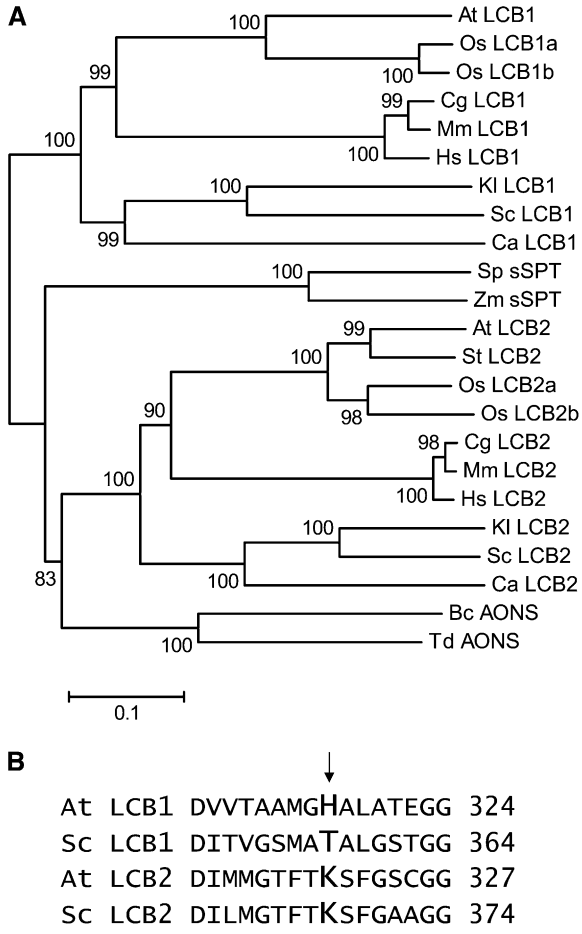

Figure 2. At LCB1 Amino Acid Sequence Phylogeny and Properties.

(A) Phylogenetic analysis of At LCB1 relative to LCB1, LCB2, and other closely related members of the α-oxoamine synthase subfamily of pyridoxal 5′-phosphate–dependent enzymes. Bootstrap values shown at nodes were obtained from 5000 trials, and branch lengths correspond to the divergence of sequences, as indicated by the relative scale. AONS, 8-amino-7-oxononanoate synthase; LCB1, SPT LCB1 subunit; LCB2, SPT LCB2 subunit; sSPT, soluble SPT. Species are as follows: At, *Arabidopsis thaliana*; Bc, *Bacillus cereus*; Ca, *Candida albicans*; Cg, *Cricetulus griseus*; Hs, *Homo sapiens*; Kl, *Kluyveromyces lactis*; Mm, *Mus musculus*; Os, *Oryza sativa*; Sc, *Saccharomyces cerevisiae*; St, *Solanum tuberosum*; Sp, *Sphingomonas paucimobilis*; Td, *Treponema denticola*; and Zm, *Zymomonas mobilis*.
(B) Comparison of the pyridoxal phosphate binding motif of LCB1 and LCB2 of *Arabidopsis* and *S. cerevisiae* SPT. The Lys (arrow) that binds pyridoxal 5′-phosphate through a Schiff's base is absent from LCB1 subunits but is present in LCB2 and other α-oxoamine synthase–related polypeptides.

synthase–related enzymes for covalent binding of the pyridoxal phosphate cofactor (Figure 2B).

Coexpression of At LCB1 and At LCB2 Complements the Long-Chain Base Auxotrophy of *S. cerevisiae lcb1*Δ and *lcb2*Δ Mutants

Yeast complementation studies were conducted to establish the function of At LCB1. A pESC-based plasmid with the At *LCB1* open reading frame fused to the *GAL1* promoter was transformed into wild-type, *lcb1*Δ, *lcb2*Δ, or *lcb1*Δ *lcb2*Δ mutant *S. cerevisiae* cells. Immunoblot analysis revealed that the At LCB1 protein was stably expressed and that it could be detected with polyclonal antibodies to the yeast LCB1 protein (Figure 3A). Consistent with its smaller size, the 482–amino acid At LCB1 protein displayed a greater electrophoretic mobility than the 558–amino acid yeast LCB1. Yeast cells lacking LCB1 and/or LCB2 require exogenous long-chain base (e.g., phytosphingosine) for growth. Although the At LCB1 protein was stably expressed, it did not eliminate the phytosphingosine dependence of the yeast *lcb1*Δ mutant (Figure 3B), indicating that it did not restore SPT activity. Because the yeast and mammalian SPT enzymes are heterodimers of the LCB1 and LCB2 subunits (Gable et al., 2002; Hanada and Nishijima, 2003), we investigated whether coexpression of the previously characterized At LCB2 (At5g23670) protein with At LCB1 would restore SPT activity to the yeast mutants. The At *LCB2* open reading frame was fused to the *GAL10* promoter in a pESC-derived plasmid that also contained the At *LCB1* cDNA under the control of the *GAL1* promoter, and expression of At LCB2 from this plasmid in yeast cells was confirmed by protein gel blot analysis with anti-At LCB2 antibodies (Figure 3A). Indeed, coexpression of At LCB1 and At LCB2 complemented the *lcb1*Δ, *lcb2*Δ, and *lcb1*Δ *lcb2*Δ mutant *S. cerevisiae* cells, allowing them to grow without exogenous phytosphingosine (Figure 3B).

The yeast *TSC3* gene encodes an 80–amino acid polypeptide that has been shown to stimulate SPT activity severalfold, and disruption of this gene results in a 10-fold decrease in SPT activity in yeast (Gable et al., 2000). In this study, deletion of the *TSC3* gene did not affect the ability of the coexpressed At LCB1/At LCB2 to rescue the long-chain base auxotrophy of the yeast *lcb1*Δ mutant (Figure 3B), and SPT activity in microsomes from this cell line also was not reduced by the lack of TSC3 (data not shown). These findings suggest that the SPT activity in yeast resulting from expression of the At LCB1 and At LCB2 subunits is not dependent on the TSC3 polypeptide.

Measurement of SPT activity in isolated microsomes from the *lcb1*Δ mutant indicated that neither At LCB1 nor At LCB2 alone has significant activity (Figure 3C), consistent with studies from yeast and mammalian cells showing that both subunits are required for SPT activity (Hanada, 2003). These data further indicate that the At LCB1 is not able to interact with the yeast LCB2 to form an active SPT enzyme. However, the yeast LCB2 protein was detected at low levels in *lcb1*Δ cells that expressed At LCB1 alone or together with At LCB2, but it was absent in vector control cells (Figure 3A). In addition, amounts of the yeast LCB2 protein were higher in cells coexpressing At LCB1 and At LCB2, which correlated with the higher levels of At LCB1 in these cells than in cells expressing only At LCB1 (Figure 3A). These observations suggest that At LCB1 interacts physically with the yeast LCB2 to stabilize this protein, but this interaction does yield detectable SPT activity (Figure 3C).

At *LCB1* Is Expressed Ubiquitously in *Arabidopsis*

Expression patterns of At *LCB1* in *Arabidopsis* were assessed by RT-PCR and by analysis of promoter–β-glucuronidase (GUS) fusions.

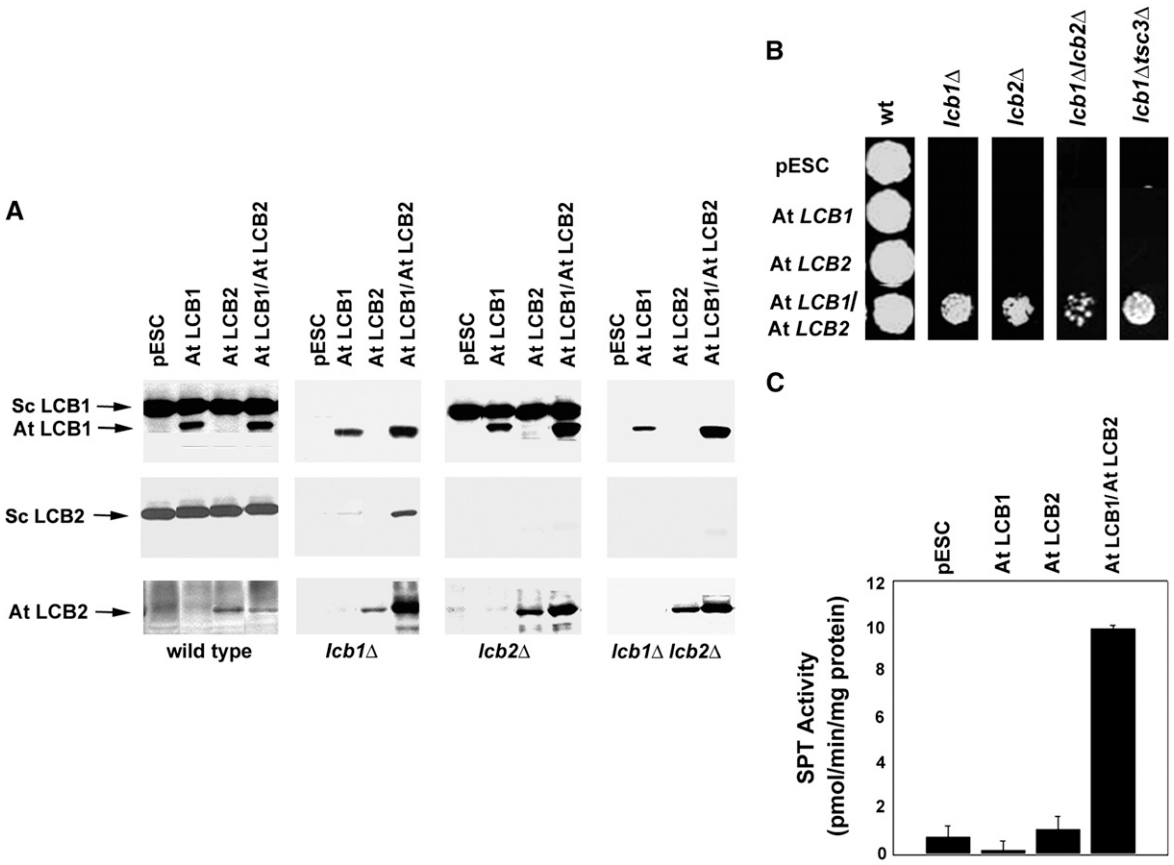

Figure 3. Coexpression of At *LCB1* and At *LCB2* Complements the Long-Chain Base Auxotrophy of *S. cerevisiae LCB1* and *LCB2* Single and Double Mutants.

(A) The At *LCB1* and At *LCB2* genes were expressed in wild-type or *lcb1Δ*, *lcb2Δ*, and *lcb1Δ lcb2Δ* mutant *S. cerevisiae* cells. Shown are immunoblots of microsomes isolated from yeast cells. The yeast LCB1 (Sc LCB1) and At LCB1 proteins were detected using a polyclonal antibody against the yeast LCB1. The yeast LCB2 (Sc LCB2) and At LCB2 polypeptides were detected using polyclonal antibodies prepared against peptides from the corresponding proteins.

(B) Growth of wild-type yeast or *lcb1Δ*, *lcb2Δ*, *lcb1Δ lcb2Δ*, and *lcb1Δ tsc3Δ* mutants expressing the At *LCB1* and At *LCB2* genes individually or together on galactose-containing medium without added phytosphingosine. pESC corresponds to cells harboring the empty expression vector.

(C) SPT activity in microsomes from yeast *lcb1Δ* cells expressing At LCB1 and At LCB2 individually or together ($n = 3$; average ± SD). For comparison, SPT activity in microsomes from wild type yeast was 100 ± 10 pmol·min^{-1}·mg^{-1} protein.

At *LCB1* mRNA was detected by RT-PCR in all *Arabidopsis* organs sampled, including young leaves, mature leaves, stems, roots, flowers, and siliques (Figure 4A). For studies with the At *LCB1* promoter, an ~2-kb sequence preceding the At *LCB1* start codon was linked with GUS and introduced into wild-type *Arabidopsis* ecotype Columbia (Col-0) plants. Consistent with the RT-PCR results, GUS activity was detected throughout the seedling and appeared to be most active in tips of the main and lateral roots (Figure 4B). GUS activity was also observed in guard cells of cotyledons (Figure 4C), mature anthers (Figure 4D), and siliques with seeds at different stages of development (Figure 4E). GUS staining of siliques was localized mainly to the central replum and the funiculus (Figure 4F). Collectively, these results indicate that At *LCB1* is expressed ubiquitously in *Arabidopsis*, consistent with the data from the microarray database (Schmid et al., 2005) (see Supplemental Figure 1 online). Expression data were also retrieved from the publicly available microarray database GENEVESTIGATOR (www.genevestigator.ethz.ch/at/; Zimmermann et al., 2004). The largest changes in expression of At *LCB1* as observed from a digital RNA gel blot containing 76 different treatments were an approximately twofold increase in response to silver nitrate and a twofold decrease in response to 2,4-D. Consistent with our results for At *LCB1*, At *LCB2* (At5g23670) was shown by Tamura et al. (2001) to be expressed in all organs of *Arabidopsis* that were examined, including leaves, stems, roots, flowers, and mature seeds. Microarray data for At *LCB2* also indicate that this gene, like At *LCB1*, is expressed ubiquitously in *Arabidopsis* (Zimmermann et al., 2004).

To examine the subcellular localization of At LCB1, binary vectors containing cauliflower mosaic virus 35S-mediated expression cassettes for a fusion protein of At LCB1–enhanced yellow fluorescent protein (EYFP) and a cyan fluorescent protein

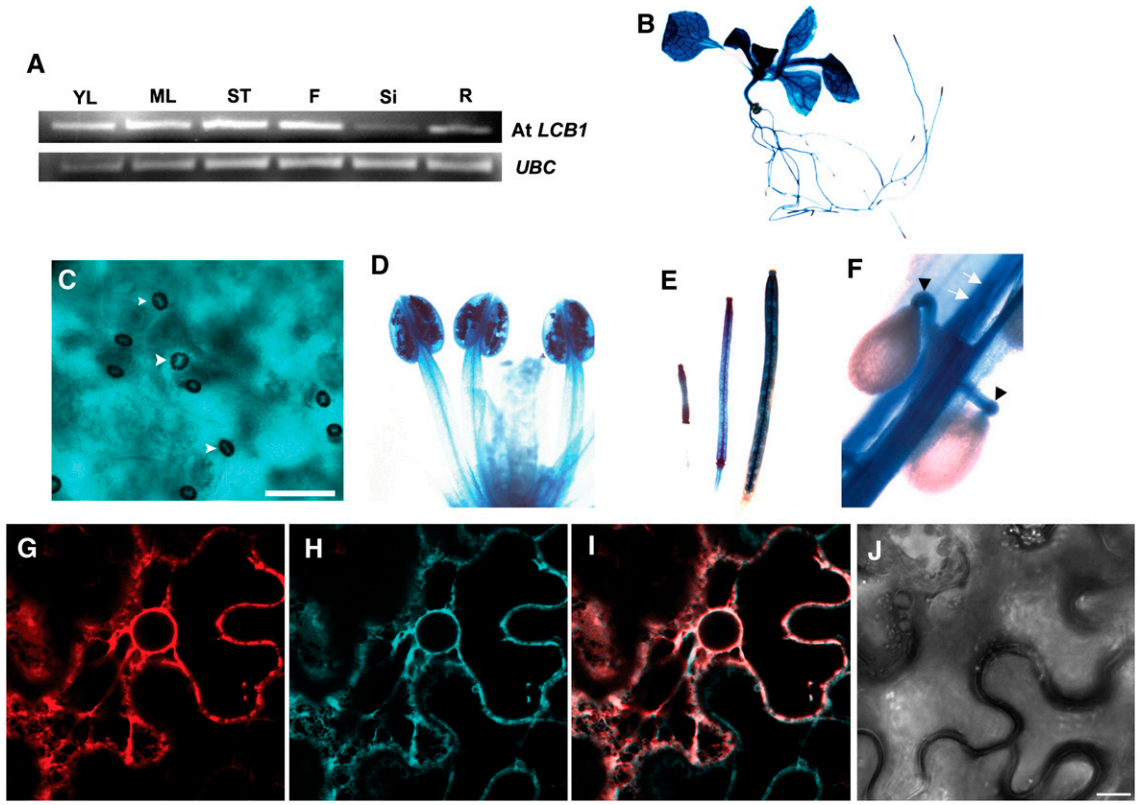

Figure 4. Expression of At *LCB1* in *Arabidopsis* and Its Subcellular Localization.

(A) RT-PCR analysis of At *LCB1* expression in young leaves (YL), mature leaves (ML), stems (ST), flowers (F), siliques (Si), and roots (R). A ubiquitin-conjugating enzyme gene (*UBC*; At5g25760) was used as an internal control.
(B) to **(F)** Localization of At *LCB1* promoter–GUS activity in *Arabidopsis* transgenic plants.
(B) Ten-day-old seedling.
(C) High expression of GUS in guard cells of cotyledons (arrowheads). Bar = 100 μm.
(D) Anthers.
(E) Siliques at 2, 4, and 7 d after flowering.
(F) GUS expression in central replum (white arrows) and funiculus (black arrowheads) from siliques at 7 d after flowering.
(G) to **(J)** Subcellular localization of At LCB1 as revealed by transient expression in tobacco leaves.
(G) Distribution of At LCB1-EYFP.
(H) Distribution of the ER marker CSP-CFP-HDEL.
(I) Merge of **(G)** and **(H)** showing colocalization of At LCB1-EYFP with the ER marker.
(J) White light image of tobacco epidermal cells. Bar = 10 μm.

(CFP)–tagged endoplasmic reticulum (ER) marker were coinfiltrated via *Agrobacterium tumefaciens* into tobacco (*Nicotiana benthamiana*) leaves. The CFP-tagged ER marker consisted of the signal peptide of basic chitinase and the HDEL ER-retention signal. Analysis of leaves from these plants by confocal microscopy revealed the colocalization of At LCB1-EYFP and the CFP signal from the ER marker (Figures 4G to 4J), indicating that At LCB1 is an ER-localized polypeptide. Similarly, GFP-tagged At LCB2 was shown previously to be ER-localized when stably expressed in tobacco BY-2 cells (Tamura et al., 2001).

T-DNA Disruption of At *LCB1* Results in Embryo Lethality

As an initial step toward the characterization of At LCB1 function in planta, T-DNA disruption mutants of At LCB1 were examined. Several potential SALK T-DNA lines (SALK_097813, SALK_097815, SALK_077745, and SALK_052712) for At *LCB1* are available (Alonso et al., 2003). In a preliminary PCR screen of these lines, a T-DNA insertion in At *LCB1* could only be confirmed in SALK_077745. The T-DNA insertion in this line was determined to be in the second intron of At *LCB1*, 214 bp downstream of the start codon (Figures 5A and 5B). This T-DNA disruption allele was designated At *lcb1-1*. The kanamycin resistance in SALK_077745 was found to be silenced, which precluded the use of antibiotic selection for the characterization of T-DNA insertion complexity in this line. However, by use of DNA gel blot analysis, only one T-DNA insertion was identified in SALK_077745 (see Supplemental Figure 2 online). In addition, 200 plants obtained from two selfed heterozygous At *lcb1-1* plants were randomly selected and genotyped by PCR. Of these plants, 62 were

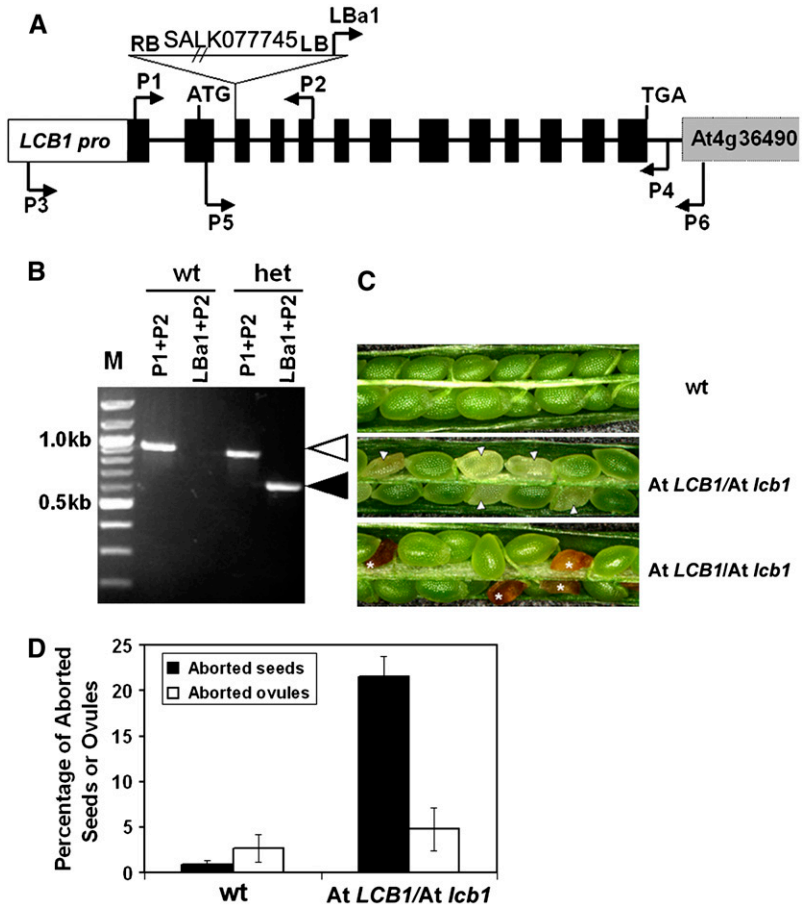

Figure 5. Gene Structure of At *LCB1* and Characterization of the At *lcb1-1* Mutant Allele.

(A) Scheme of At *LCB1*. The predicted At *LCB1* open reading frame contains 13 exons (black boxes) and 12 introns (black lines). The At *LCB1* promoter (*LCB1 pro*) and neighboring gene (At4g36490) are also shown. The T-DNA insert in SALK_077745 (indicated by the inverted triangle) is located in intron 2 and has the same orientation to the At *LCB1* gene. The primers shown were used to determine the location of the T-DNA insertion, to amplify the genomic sequence for complementation experiments, and to verify the complementation of the SALK_077745 mutant.

(B) PCR genotyping of SALK_077745 T-DNA lines. PCR was conducted with genomic DNA from a population of SALK_077745 T4 plants using a pair of At *LCB1*–specific primers (P1 and P2) or by the combination of T-DNA left border–specific primers (LBa1) and a corresponding At *LCB1*–specific primer (P2). In wild-type plants, only the wild-type allele (indicated by an ~900-bp band; white arrowhead) was amplified, and no T-DNA allele was detected. However, in the heterozygous At *LCB1-1* (het) plants, both the wild-type allele (~900 bp) and the T-DNA disruption allele (indicated by an ~600-bp band; black arrowhead) were amplified.

(C) Morphology of seeds from wild-type (Col-0) and heterozygous At *lcb1-1* plants. Shown are siliques from a wild-type plant (top panel) and from heterozygous At *lcb1-1* plants at 7 to 10 d after flowering (middle panel) and 14 d after flowering (bottom panel). The aborted seeds are either pale (arrowheads) or brown and shrunken (asterisks), depending upon the maturity of seeds.

(D) Average percentage of aborted seeds and ovules from siliques of wild-type (Col-0) and selfed heterozygous At *LCB1*/At *lcb1* plants. The average number of aborted seeds and ovules from 10 siliques collected from five plants and the SD are presented ($n = 5$; >500 total seeds were examined). Ovule abortion was assessed as described previously (Meinke, 1994).

determined to be wild type and 138 were determined to be heterozygous for At *lcb1-1*, which corresponded to a ratio of ~1:2. Plants homozygous for At *lcb1-1* were not found. Notably, the heterozygous At *lcb1-1* plants were indistinguishable from wild-type plants under the growth conditions used in these studies. However, analysis of siliques from the heterozygous At *lcb1-1* lines revealed a substantial increase in the number of aborted seeds relative to siliques from the wild-type plants (Figure 5C).

Seed abortion in plants heterozygous for At *lcb1-1* was examined further in siliques collected from 7 to 10 d after flowering. At this stage, seeds with a white translucent appearance that lacked a developing embryo were observed at an increased frequency in siliques from heterozygous At *lcb1-1* plants relative to those from wild-type plants. By contrast, seeds with a properly developing embryo were green and round. At later stages of development, these aberrant seeds were brown and shrunken (Figure 5C). To quantify this phenotype, >500 seeds from 10

siliques were examined. Approximately 25% of seeds from the heterozygous At *lcb1-1* plants and 1% of seeds from wild-type plants were aborted (Figure 5D). Collectively, (1) the inability to obtain homozygous At *lcb1-1* plants, (2) the observed 1:2 segregation of wild-type and heterozygous progeny from selfed At *LCB1*/At *lcb1* plants, and (3) the high frequency of aborted seeds in siliques from heterozygous At *lcb1-1* plants indicated that disruption of At *LCB1* is lethal. No significant reduction in pollen viability (data not shown) and little or no increase in ovule abortion was observed in the heterozygous At *lcb1-1* plants (Figure 5D). Consistent with this finding, reciprocal crosses revealed that transmission of the mutant allele through male and female gametophytes was unaffected (data not shown).

To conclusively demonstrate that seed abortion is caused by the disruption of At *LCB1*, experiments were conducted to determine whether this phenotype could be rescued by the expression of a wild-type At *LCB1* transgene. For these complementation studies, an ~5-kb genomic copy of At *LCB1* (containing its native promoter) was transformed along with a glufosinate resistance marker into heterozygous At *lcb1-1* plants. PCR-based screening using primers P5 and P6 (Figure 5A) was conducted on 30 of the resulting T1 glufosinate-resistant transformants. Seven of these 30 transformants lacked a chromosomal copy of the wild-type At *LCB1* allele and therefore were homozygous for the At *lcb1-1* mutation. Seed abortion frequency was also examined in two heterozygous At *lcb1-1* mutant plants that carried genomic At *LCB1* transgenes. Of >500 seeds analyzed from both plants, the seed abortion frequency was 5.2% in one plant and 6.9% in the second plant. These numbers are consistent with the 6.25% seed abortion rate that would be expected for a single-copy At *LCB1* transgene in a heterozygous At *lcb1-1* T-DNA mutant background. These data conclusively demonstrate that the seed abortion phenotype observed in the At *lcb1-1* T-DNA mutant results from the disruption of the At *LCB1* gene and can be rescued by expression of a wild-type copy of this gene.

To more clearly define the nature and timing of seed abortion in At *lcb1-1* mutants, differential interference contrast microscopy was conducted on developing seeds from wild-type and heterozygous At *lcb1-1* plants upon clearing of dissected seeds with Hoyer's reagent (Meinke, 1994). This method allowed us to more easily distinguish early events that lead to seed abortion that could not be detected by empirical analyses of dissected seeds. At very early stages of seed development, homozygous At *lcb1-1* seeds were visually indistinguishable from other seeds in the same siliques, but at later stages of development, approximately one-fourth of the seeds from heterozygous At *lcb1-1* plants were brown and shrunken (Figure 5C). Based on the segregation and complementation studies described above, these seeds corresponded to the homozygous At *lcb1-1* state. (The inability to cleanly dissect embryos from these seeds precluded the use of PCR to directly confirm their genotype.) Using differential interference contrast microscopy, the growth of embryos from homozygous At *lcb1-1* seeds was observed to arrest at early stages of development. In this regard, embryo development of homozygous At *lcb1-1* seeds was apparently disrupted before the globular stage. Approximately three-fourths of the seeds obtained at 2 d after flowering from siliques of heterozygous At *lcb1-1* plants contained a normal globular embryo with an extended suspensor (Figure 6A). However, approximately one-fourth of these seeds contained embryos with an aberrant appearance (Figures 6B to 6D). These embryos did not arrest at a single developmental point, as indicated by the presence of embryos with one (Figure 6B), two (Figure 6C), or multiple (Figure 6D) cells. Regardless of the cell numbers, these embryos contained abnormal cell patterns, and the suspensors were severely reduced in length (Figure 6D) relative to embryos with a normal appearance (Figure 6A). Although the normal embryos continued

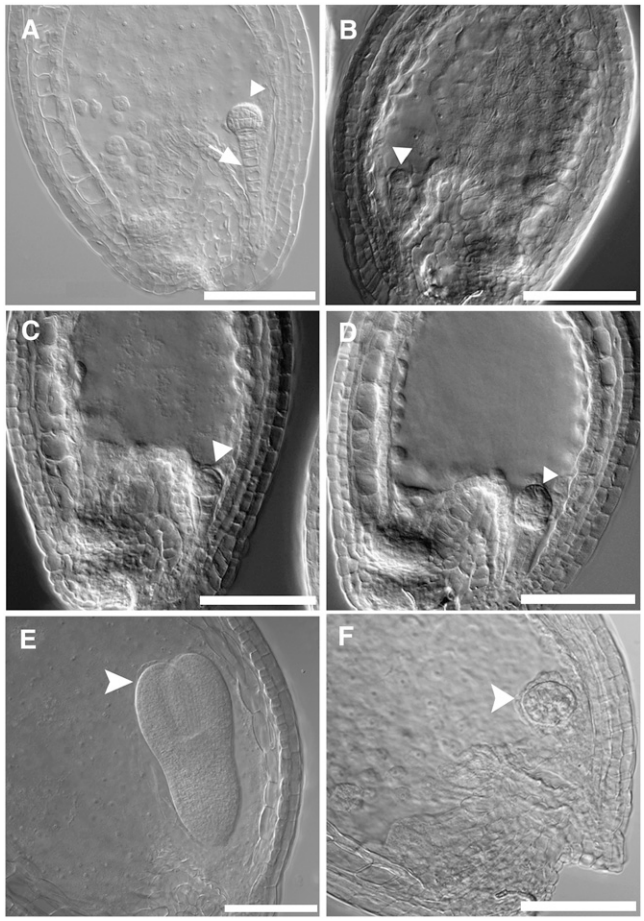

Figure 6. Defective Embryo Development is Observed in Homozygous At *lcb1-1* Seeds.

(A) Wild-type seed (2 d after flowering) showing a globular embryo (arrowhead) and an extended suspensor (arrow).
(B) to **(D)** Aberrant embryos observed in homozygous At *lcb1-1* seeds. The homozygous segregants were dissected from siliques collected at 2 d after flowering from selfed heterozygous At *lcb1-1* plants.
(B) Embryo arrested at the one-cell stage.
(C) Embryo arrested at the two-cell stage.
(D) Early globular embryo with an abnormal cell pattern and a shortened suspensor.
(E) Wild-type embryo at the torpedo stage (4 to 5 d after flowering).
(F) Residue of a degenerated embryo from a homozygous At *lcb1-1* seed (4 to 5 d after flowering).
Bars = 100 μm.

to develop to the torpedo stage (Figure 6E), embryos from homozygous At *lcb1-1* seeds did not reach the full globular stage, and in some cases degeneration of the embryo was observed (Figure 6F).

RNA Interference Suppression of At *LCB1* Results in Plants with Reduced Size and Altered Leaf Morphology

RNA interference (RNAi) experiments were conducted to determine the effects of the partial suppression of At *LCB1* expression on plant growth and development and on sphingolipid metabolism. For these studies, a pHellsgate8-based (Helliwell and Waterhouse, 2003) RNAi construct was prepared from a 319-bp portion of the At *LCB1* open reading frame and introduced into wild-type *Arabidopsis* (Col-0). Fifty independent kanamycin-resistant lines were obtained from this transformation and designated LCB1i-*x* (where *x* corresponds to the transgenic event number). The transformants displayed two distinct phenotypes. One group of plants (21 of 50 total transformants) was markedly reduced in size relative to wild-type plants and had curled rosette and cauline leaves and thin stems (Figure 7A). The second group of transformants (29 of 50 total transformants) was indistinguishable from wild-type plants. Ten independent lines from each group were selected for further RT-PCR analysis, and the results indicated that plants from the first group had reduced expression of At *LCB1* relative to wild-type controls, whereas plants from the second group did not have a detectable change in At *LCB1* expression. An example of mRNA expression levels detected in three plants from each group is shown in Figure 7B. The differences in growth and At *LCB1* expression between the two groups of plants were maintained in the T2 generation. Real-time PCR was conducted to quantify the reduction in At *LCB1* expression in plants with altered growth and morphology. In plants from three independent lines, mRNA levels of At *LCB1* were 20 to 40% of those from wild-type plants of similar age (Figure 7C). Similar phenotypes, including reduction in the size of plants and curled leaf morphology, were also observed with At *LCB1* RNAi lines produced by use of a pHannibal-based construct generated from the same portion of the At *LCB1* open reading frame. In addition, crosses of the T1 At *LCB1* RNAi plants with wild-type Col-0 yielded plants with reduced size and altered leaf morphology in approximately half of the offspring (data not shown), indicating that these phenotypes are dominantly conferred by the At *LCB1* RNAi transgene. This was confirmed by an

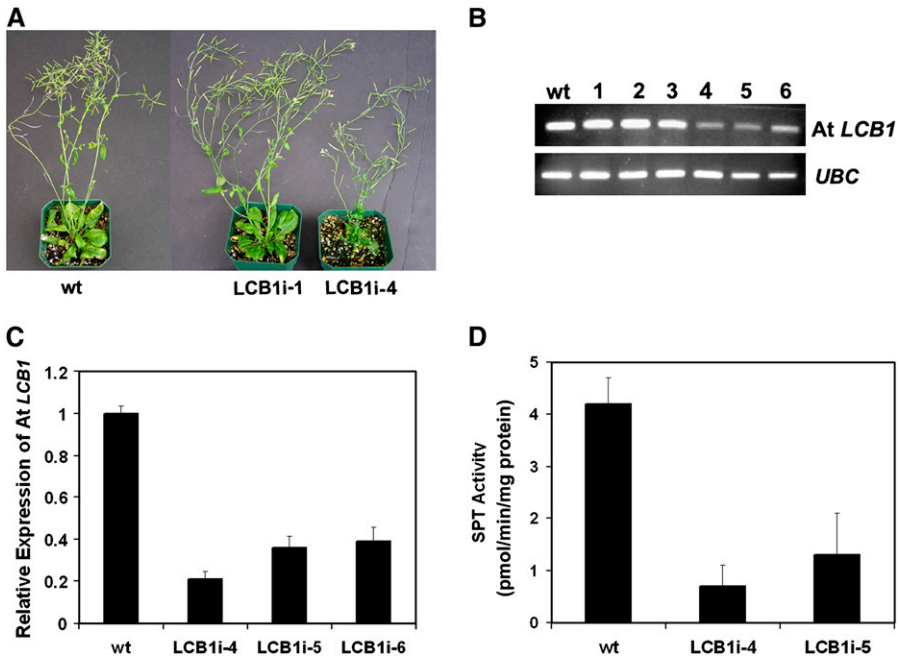

Figure 7. RNAi-Mediated Suppression of At *LCB1* Results in Distinct Growth Phenotypes That Correlate with the Relative Degree of Reduced At *LCB1* Expression.

(A) Two phenotypic classes were observed in T1 At *LCB1* RNAi plants: one class that was indistinguishable from wild-type plants, as represented by LCB1i-1, and a second class with reduced overall size and curled leaves, as represented by LCB1i-4.

(B) RT-PCR analyses of wild-type and representative At *LCB1* RNAi suppression lines. Plants indistinguishable from wild-type plants had no detectable reduction in At *LCB1* expression (lanes 1 to 3), whereas small plants with altered leaf morphology displayed reduced expression of At *LCB1* (lanes 4 to 6). A gene for a ubiquitin-conjugating enzyme (see Methods) was used as an internal control.

(C) Real-time PCR quantification of At *LCB1* expression T2 plants from At *LCB1* suppression lines. Expression of At *LCB1* was normalized relative to the expression of a ubiquitin-conjugating enzyme gene. Results from three independent experiments are presented as averages ± SD.

(D) SPT activity in microsomes from leaves of wild-type (Col-0) and LCB1i-4 and LCB1i-5 RNAi plants ($n = 3$; average ± SD).

~3:1 segregation of small plants to normal-size plants among the T2 seedlings that were obtained from selfed T1 At *LCB1* RNAi plants (data not shown).

The lack of a suitable antibody for the detection of At LCB1 in plant extracts (see Methods) precluded measurement of the levels of this polypeptide in RNAi and wild-type lines. As an alternative approach, SPT activity was determined in microsomal extracts from leaves of wild-type plants and three independent At *LCB1* RNAi lines, two pHellsgate8-based RNAi lines, and a pHannibal-based RNAi line. SPT activities from the wild-type plants and the two pHellsgate8-based RNAi lines are shown in Figure 7D, and SPT activity from the pHannibal-based RNAi line was 0.37 ± 0.21 pmol·min^{-1}·mg^{-1} protein. SPT activity in leaf microsomes from RNAi lines was reduced by 4- to 10-fold relative to that detected in leaf microsomes from wild-type plants.

The LCB1i-4 RNAi suppression line was chosen for detailed phenotypic analyses, as described below. However, it should be noted that similar alterations in plant morphology and sphingolipid composition as those reported below were observed in multiple, independent transformation events and in lines obtained from the pHannibal-based RNAi construct.

Sphingolipid Composition, but Not Content, Is Altered by RNAi Suppression of At *LCB1*

Given that At LCB1 is a subunit of SPT, which catalyzes the first step in sphingolipid biosynthesis, we hypothesized that partial suppression of At *LCB1* expression by RNAi would result in reduced sphingolipid content in plants. To test this hypothesis, the total long-chain base composition was measured in lyophilized leaves from 4-week-old wild-type and RNAi-suppression LCB1i-4 plants. Long-chain bases are components of all sphingolipids and are unique to this lipid class. Therefore, measurement of total long-chain base content in leaves directly reflects the total sphingolipid content of these organs. Surprisingly, no significant difference was detected in the long-chain base content of leaves from wild-type (1.82 ± 0.38 nmol/mg dry weight) and LCB1i-4 (1.88 ± 0.39 nmol/mg dry weight) plants on a weight basis (Figure 8A).

Measurement of the sphingolipid long-chain base composition, however, revealed large increases in the relative amounts of saturated trihydroxy and dihydroxy long-chain bases in leaves from LCB1i-4 plants compared with those from wild-type plants. Most notably, relative amounts of phytosphingosine (t18:0) increased from ~6 to 8% in leaves of wild-type plants to 20 to 30% in leaves of LCB1i-4 plants (Table 1). A similar level of increase was also detected in relative amounts of dihydrosphingosine (d18:0) between leaves of wild-type and LCB1i-4 plants (Table 1).

To determine whether increases in saturated long-chain bases occur broadly in sphingolipid classes in LCB1i-4 plants, sphingolipids were fractionated into charged and neutral fractions based on their affinity for a weak anion-exchange resin (Markham et al., 2006). As described recently, the charged fraction is composed primarily of glycosylated inositolphosphoceramides, and the neutral fraction is composed principally of monoglucosylceramides, which were further purified for these studies, and lesser amounts of free ceramides (Markham et al., 2006). Interestingly, increases in relative amounts of saturated long-chain bases in leaves of LCB1i-4 were observed primarily in the charged sphingolipid fraction as well as in the tissue residue that contained nonextracted sphingolipids (Figures 8C and 8D). By contrast, only very small amounts of the saturated long-chain bases phytosphingosine and dihydrosphingosine were detected in monoglucosylceramides from leaves of either the wild type or the RNAi suppression line (Figure 8E).

Cell Expansion Is Affected in Plants with Partial Suppression of At *LCB1* Expression

As described above, the most notable phenotypic differences between wild-type and At *LCB1* RNAi suppression plants in the T1 generation were the overall size of the plants and the leaf shape (Figure 7A). These phenotypes were maintained in T2 RNAi plants, and a detailed comparison with wild-type plants was conducted. As shown in Figures 9A and 9B, 4-week-old T2 plants from the RNAi suppression line LCB1i-4 were approximately one-third the size of wild-type plants of the same age. This size difference was accentuated when plants were maintained under a short-day regime (data not shown), and the smaller size of LCB1i-4 plants was observed throughout their development. LCB1i-4 plants were also found to have smaller leaves and shorter petioles than wild-type plants (Figures 9C and 9D). Interestingly, the leaf blades were curled, and the leaf tip was twisted slightly to form a flag-like projection at the ends of leaves (Figure 9D, arrow). In addition, necrotic lesions were often observed on mature rosette leaves of LCB1i-4 plants, which initially appeared on the adaxial (upper) surfaces (Figure 9E). Because both the leaf blade and petiole of LCB1i-4 plants were smaller than those of wild-type plants (Figures 9C and 9D), we hypothesized that reduced sphingolipid synthesis resulting from partial suppression of At *LCB1* expression limits the ability of cells to expand, as has been shown for *Arabidopsis cer10* mutants (Zheng et al., 2005). To address this possibility, mesophyll cells from the petiole and pavement cells from the abaxial leaf surface of wild-type and LCB1i-4 plants were examined by microscopy. Mesophyll cells in the LCB1i-4 petioles were approximately one-third the length of equivalent cells in wild-type plants of the same age (Figure 9F), which was proportional to the reduction in the overall size of these plants. Pavement cells in LCB1i-4 plants were also markedly smaller than those in wild-type plants (Figures 9G and 9H). We also observed that trichomes of the LCB1i-4 plants were shorter, but their morphology was not altered (data not shown). Overall, these observations indicate that the smaller size of the LCB1 RNAi plants is attributable primarily to reduced cell expansion.

DISCUSSION

SPT catalyzes the first step in the synthesis of long-chain bases, the signature components of all sphingolipids (Sperling and Heinz, 2003). In this report, we have demonstrated that At *LCB1* (At4g36480) encodes a genuine LCB1 subunit of SPT, and we have shown that plant SPT functions as a heteromeric enzyme that requires both LCB1 and LCB2 for activity. This subunit composition is similar to what has been reported for yeast (Gable

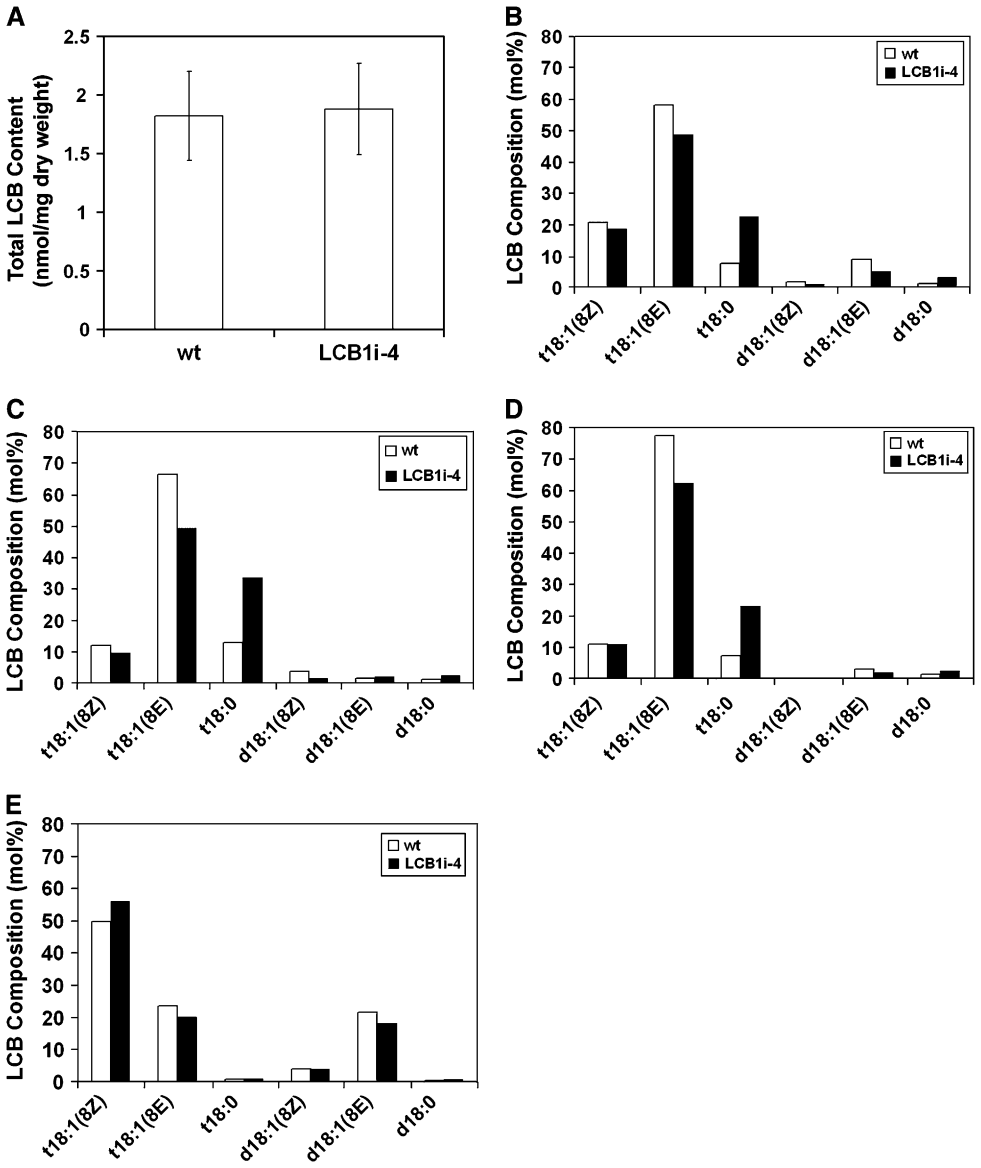

Figure 8. Effects of At *LCB1* RNAi Suppression on Sphingolipid Long-Chain Base Content and Composition.

(A) Total sphingolipid long-chain base content of leaves from wild-type and LCB1i-4 RNAi suppression plants ($n = 10$; average ± SD).

(B) Long-chain base composition of sphingolipids in the total solvent extract from leaves of wild-type and LCB1i-4 plants. Data in **(B)** to **(E)** are representative of three independent experiments.

(C) Long-chain base composition of sphingolipids in the tissue residue after solvent extraction from leaves of wild-type and LCB1i-4 plants.

(D) Long-chain base composition of charged sphingolipids from leaves of wild type and LCB1i-4 plants. This fraction is composed primarily of glycosylated inositolphosphoceramides (Markham et al., 2006).

(E) Long-chain base composition of monoglucosylceramides from leaves of wild-type and LCB1i-4 plants.

et al., 2000) and mammalian cells (Hanada et al., 2000), but it is different from the homodimeric form of SPT described in *Sphingomonas* species (Ikushiro et al., 2001). In addition, we have shown that T-DNA disruption of At *LCB1* results in embryo lethality. Because SPT mediates the initial reaction in sphingolipid biosynthesis, this result indicates that sphingolipids are required for the viability of *Arabidopsis*, which to our knowledge is the first direct demonstration that sphingolipids are essential components of plant cells. Furthermore, we show that partial suppression of At *LCB1* expression by RNAi is accompanied by altered leaf morphology and a dwarfing phenotype that results primarily from reduced cell expansion. These plants displayed little change in the total sphingolipid long-chain base content when measured on a weight basis, which suggests that plants adjust their growth to compensate for the reduced availability of sphingolipids.

Table 1. Sphingolipid Long-Chain Base Composition of Leaves from Wild-Type (Col-0) and LCB1i-4 RNAi Suppression Plants

Plant	t18:1(*Z*)	t18:1(*E*)	t18:0	d18:1(*Z*)	d18:1(*E*)	d18:0
Wild type	19.6 ± 1.0	64.2 ± 3.2	6.0 ± 0.8[a]	1.2 ± 0.3	7.6 ± 1.8	1.0 ± 0.3[a]
LCB1i-4	14.1 ± 1.2	48.2 ± 3.3	27.5 ± 4.5[a]	0.9 ± 0.2	5.0 ± 1.4	4.5 ± 0.7[a]

Values shown are mol %. Each value is the mean of 10 independent measurements ± SD. t18:1(*E* or *Z*), 4-hydroxy-8-(*trans* or *cis*)-sphingenine; t18:0, 4-hydroxysphinganine or phytosphingosine; d18:1(*E* or *Z*), 8-(*trans* or *cis*)-sphingenine; d18:0, sphinganine or dihydrosphingosine.
[a] Student's *t* test indicated that both t18:0 and d18:0 are significantly increased in LCB1i-4 plants compared with wild-type plants ($P < 0.001$).

The Subunit Structure of *Arabidopsis* SPT as Revealed by Yeast Complementation Is Similar to That of Other Eukaryotes

Functional identification of the At LCB1 polypeptide is problematic because this polypeptide is not catalytic on its own as a result of the absence of an active site Lys that is required for the binding of pyridoxal phosphate, an essential cofactor for SPTs and other α-oxoamine synthases (Figure 2B). The lack of an active site Lys in At LCB1 is a property that is shared with other eukaryotic LCB1 polypeptides (Hanada, 2003). In these SPTs, the catalytic pyridoxal phosphate binding domain instead resides in the LCB2 subunit. Although LCB1 is required for SPT activity, its specific function in SPT catalysis is not well defined. LCB1 is required for the stabilization of LCB2, and immunoprecipitation experiments have demonstrated that the structure of the yeast enzyme is an LCB1/LCB2 heterodimer (Gable et al., 2000). Similarly, immunoprecipitation of LCB1 from CHO cell extracts coprecipitates LCB2 in equimolar amounts (Hanada et al., 2000). Furthermore, the crystal structure of AONS (Alexeev et al., 1998), an α-oxoamine synthase enzyme that is nearly as related to LCB1 as LCB1 and LCB2 are to each other (Figure 2A), provides important insights. In particular, AONS is a head-to-tail homodimer that has two symmetrical active sites formed at the interface between the subunits, with residues from each subunit participating in pyridoxal phosphate binding (Alexeev et al., 1998). Mutational and structural studies of yet another α-oxoamine synthase, aminolevulinate synthase, also indicate that the enzyme is a head-to-tail homodimer with two symmetrical active sites lying at the interface of the subunits and with both subunits having residues that participate in catalysis (Gong et al., 1996; Astner et al., 2005). By analogy and based on modeling and mutational studies, SPT has been proposed to be a head-to-tail heterodimer of LCB1 and LCB2 with a single active site at the interface made up of residues from both LCB2 (including the active site Lys) and LCB1 (Gable et al., 2002).

In this study, the functional identity of At LCB1 was established through complementation assays using *S. cerevisiae* sphingolipid long-chain base auxotrophs that carry disruptions in the *LCB1* and/or *LCB2* genes. Yeast complementation has previously been of limited value for the characterization of LCB1 or LCB2 subunits from other organisms. For example, expression of the mouse LCB2 (Nagiec et al., 1996) or the previously described At LCB2 in *LCB2* mutants of *S. cerevisiae* (Tamura et al., 2001) did not result in the complementation of the long-chain base auxotrophy. One interpretation of these results was that proteins encoded by the heterologous LCB2s were unable to productively interact with the *S. cerevisiae* LCB1 to generate sufficient SPT activity for complementation. In this study, we were only able to complement *S. cerevisiae* SPT mutants by the expression of At LCB1 together with At LCB2. Not only did this result conclusively establish that At LCB1 is a component of the *Arabidopsis* SPT, but it also showed that SPT in *Arabidopsis* and likely all plants is a heteromeric enzyme. Of note, complementation of *S. cerevisiae* SPT mutants by coexpression of heterologous LCB1 and LCB2 polypeptides from any source has not been described previously. The ability to functionally express At LCB1 and At LCB2 in a background devoid of any SPT activity should provide a useful model system for more detailed characterization of the biochemical and membrane topological properties of the *Arabidopsis* SPT.

The SPT activity from coexpression of the *Arabidopsis* polypeptides was ~10-fold lower than the SPT activity from microsomes of wild-type *S. cerevisiae*. In this regard, it is notable that the 80–amino acid Tsc3 protein has been shown to stimulate SPT activity in *S. cerevisiae* (Gable et al., 2000). An analogous protein has yet to be identified in any other organism. It is possible that a Tsc3-like polypeptide from *Arabidopsis* is necessary to achieve optimal SPT activity from At LCB1/At LCB2 coexpression in *S. cerevisiae*.

Sphingolipids Are Essential for the Viability of *Arabidopsis*

Because SPT catalyzes the committed step of sphingolipid biosynthesis, our inability to recover homozygous T-DNA disruption mutants for At *LCB1* indicates that sphingolipids are essential for the viability of *Arabidopsis*. This conclusion is also supported by results from parallel studies of At *LCB2* T-DNA mutants (C.R. Dietrich and E.B. Cahoon, unpublished results). Although this is not an unexpected finding, no direct evidence has been reported previously to show that sphingolipids are required by plants. The isolation of mutants for SPT subunit genes previously established that sphingolipids are essential in yeast (Buede et al., 1991), CHO cells (Hanada et al., 1992), mouse (Hojjati et al., 2005), and *Drosophila* (Adachi-Yamada et al., 1999) and are required for the differentiation of the protozoan *Leishmania major* (Zhang et al., 2003). Several chemical inhibitors of SPT do exist, including cycloserine, myriocin, and sphingofungin B (Dickson, 1998). Cycloserine, for example, has been shown to strongly inhibit SPT activity in squash fruit (*Cucurbita pepo*) microsomes (Lynch and Fairfield, 1993), and myriocin was used to inhibit de novo sphingolipid synthesis in labeling studies conducted with tomato (*Solanum lycopersicum*) leaves (Spassieva et al., 2002). However, the use of these inhibitors to show that sphingolipids are essential in plants has not been described

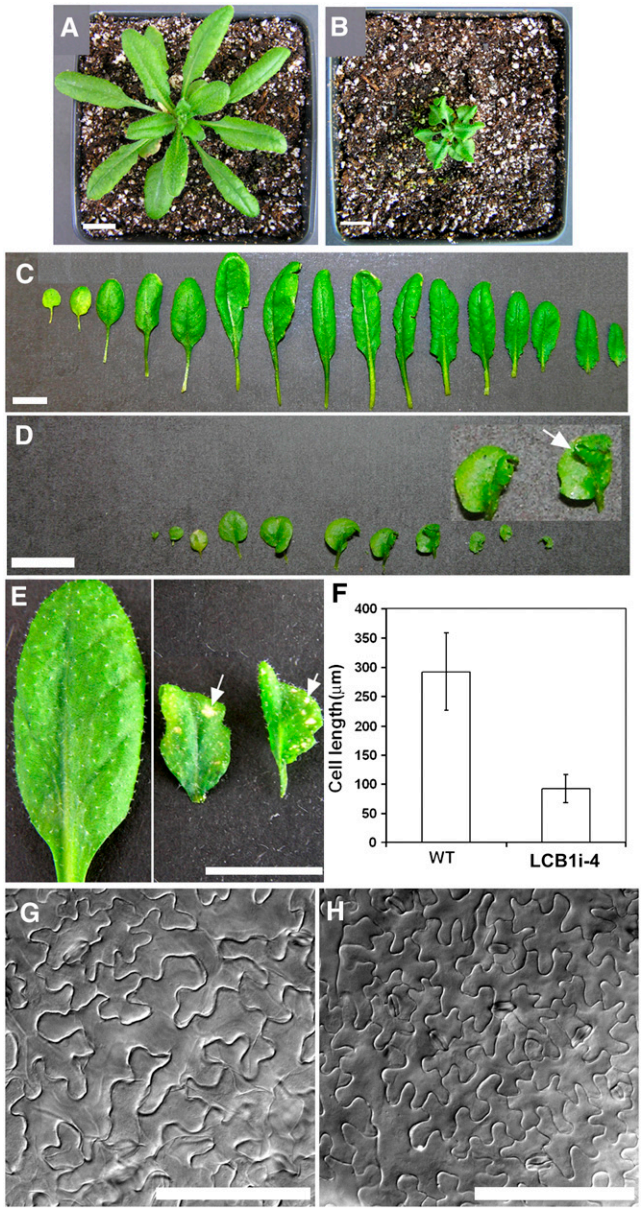

Figure 9. RNAi-Mediated Suppression of At *LCB1* Expression Results in Reduced Sizes of Plants and Cells and Altered Leaf Morphology.

The data shown are from the LCB1i-4 line. Similar results were obtained with pHannibal-based At *LCB1* RNAi lines.

(A) and **(B)** Four-week-old wild-type **(A)** and LCB1i-4 RNAi suppression **(B)** plants.

(C) Arrangement of all leaves from a 4-week-old wild-type plant.

(D) Arrangement of all leaves from a 4-week-old LCB1i-4 plant. The inset shows an enlargement of leaves that display altered shape.

(E) Lesion-like spots were often observed on leaves of LCB1i-4 plants (right panel; arrows). These spots were absent from leaves of wild-type plants (left panel).

(F) Cell length of mesophyll cells from the petiole of the fifth rosette leaf of 4-week-old wild type and LCB1i-4 plants ($n = 120$; average ± SD).

(G) and **(H)** Pavement cells of the abaxial leaf surface from wild-type **(G)** and LCB1i-4 **(H)** plants.

Bars = 1 cm in **(A)** to **(E)** and 100 μm in **(G)** and **(H)**.

previously. In addition, it is well known that inhibitors of ceramide synthesis (e.g., fumonisins and AAL toxin) induce programmed cell death in plants, but this effect is believed to result primarily from the buildup of cytotoxic long-chain bases or long-chain base derivatives (Wang et al., 1996; Asai et al., 2000; Spassieva et al., 2002; Gechev et al., 2004).

The lethality associated with At *LCB1* T-DNA disruption was observed primarily during embryo development. Approximately 25% of the embryos in seeds from heterozygous At *lcb1-1* plants were observed to arrest at the globular stage of development, which was followed in some seeds by apparent disintegration of the embryo. By contrast, At *LCB1* disruption had little or no effect on pollen or ovule viability. In addition, reciprocal cross results between heterozygous At *lcb1-1* and the wild type (Col-0) demonstrated normal transmission of the mutant allele through both male and female gametophytes (data not shown). The apparent absence of gametophytic lethality from At *LCB1* T-DNA disruption was surprising given the likely requirement for sphingolipids in pollen and ovules. Lack of gametophytic lethality, however, is often observed in T-DNA mutants for essential genes (Bonhomme et al., 1998). One possible explanation for the absence of gametophytic lethality in the At *LCB1* T-DNA disruption mutant is that sphingolipids, At LCB1 protein, or At *LCB1* mRNA is transmitted from the sporophytic maternal cells at levels sufficient to support the viability of gametes. We also cannot rule out the possibility that a low level of wild-type At *LCB1* expression occurs from the T-DNA disruption locus, given that the T-DNA insertion resides within an intron. Because sphingolipids are major structural components of plasma membrane and tonoplast (Yoshida and Uemura, 1986; Lynch and Steponkus, 1987; Sperling et al., 2005), it is likely that embryo lethality from At *LCB1* T-DNA disruption results largely from losses in membrane integrity. Sphingolipids are also enriched in detergent-resistant membranes (or lipid rafts) isolated from plasma membrane (Mongrand et al., 2004; Borner et al., 2005). As such, it is also possible that the loss of sphingolipid biosynthetic ability leads to alterations in the organization and function of plasma membrane–associated proteins, including glycosylphosphatidylinositol-anchored proteins and several proton ATPases that have been identified in lipid raft structures from *Arabidopsis* (Borner et al., 2005). Furthermore, the possibility that sphingolipid-derived signaling molecules, including long-chain base phosphates, play an essential role in embryogenesis cannot be excluded (Ng et al., 2001; Coursol et al., 2003, 2005; Spiegel and Milstien, 2003; Imai and Nishiura, 2005).

Downregulation of Sphingolipid Biosynthesis by RNAi Suppression of At *LCB1* Results in Altered Growth and Development of *Arabidopsis*

The use of RNAi allowed us to examine the effects of partial, nonlethal reductions in At *LCB1* expression on plant growth and development and on the content and composition of sphingolipids. Plants with obvious growth phenotypes obtained from these experiments displayed a 60 to 80% reduction in At *LCB1* expression level. Plants with more complete reductions in At *LCB1* expression were not recovered, consistent with our conclusion from the T-DNA mutant study that sphingolipids are

essential for the viability of *Arabidopsis*. Dwarfing was the most marked phenotype displayed by plants with partially suppressed At *LCB1* expression. Although it cannot be ruled out that cell division was affected, the small size of plants appeared to be attributable mostly to reduced cell expansion. This was exemplified by the smaller size of abaxial epidermal pavement cells and by the threefold reduction in the length of mesophyll cells of the petiole in At *LCB1* RNAi plants (Figures 9F to 9H). Recently, *Arabidopsis cer10* mutants, which have decreased levels of very-long-chain fatty acids in waxes, triacylglycerols, and sphingolipids, were shown to have a dwarfing phenotype similar to that of At *LCB1* RNAi plants (Zheng et al., 2005). In addition, *cer10* mutants have curled leaves, which are also observed in At LCB1 RNAi plants. It was speculated that these growth and development phenotypes in *cer10* mutants are attributable to observed alterations in sphingolipid-associated endocytotic membrane trafficking (Zheng et al., 2005). It is possible that these alterations may also occur in response to reduced rates of sphingolipid synthesis that result from RNAi suppression of At *LCB1*.

Despite the dwarfing and other phenotypes resulting from RNAi suppression of At *LCB1*, we were unable to detect a significant change in the sphingolipid long-chain base content on a per weight basis in leaves of these plants relative to those of nontransformed control plants. This result suggests that the reduced growth of these plants may be a compensatory response to limitations in the availability of sphingolipids for membranes. Given that sphingolipids are essential molecules, as shown by the At *LCB1* T-DNA mutant studies, such a result may not be unexpected, and similar results have been observed for SPT defects in other organisms. For example, CHO cells with temperature-sensitive mutations in SPT displayed reduced growth when maintained under nonpermissive conditions, but growth was restored when sphingolipid long-chain bases were provided exogenously (Hanada et al., 1992). Unexpected, however, was the increase in relative levels of saturated long-chain bases (i.e., phytosphingosine [t18:0] and dihydrosphingosine [d18:0]) in leaves of the At *LCB1* RNAi plants, which was observed primarily in a fraction enriched in glycosylated inositolphosphoceramides. This finding is likely attributable to alterations in Δ^8 desaturation of long-chain bases, because this effect was observed with both trihydroxy and dihydroxy long-chain bases. Although a number of possible explanations can be proposed, an intriguing hypothesis is that downregulation of sphingolipid synthesis via the suppression of At *LCB1* results in reduced flux of long-chain bases or complex sphingolipid precursors to intracellular sites of Δ^8 desaturation because of disruptions in sphingolipid-mediated membrane trafficking, as described for the *Arabidopsis cer10* mutant (Zheng et al., 2005).

At *LCB1* RNAi Plants and *fatb* Mutants Share Some Phenotypic Similarities

It is notable that several of the phenotypic alterations in At *LCB1* RNAi plants are also observed in *fatb* mutants (Bonaventure et al., 2003), although the magnitude of these alterations was more severe in plants with reduced At *LCB1* expression. These similarities include the reduced size of plants and an increase in relative amounts of phytosphingosine (Bonaventure et al., 2003). *fatb* mutants produce lower amounts of palmitic acid because of lesions in the gene for the FATB-type acyl-acyl carrier protein thioesterase. The CoA ester of palmitic acid is one of the substrates of SPT (Figure 1). It was speculated, among several possibilities, that the smaller size of *fatb* mutant plants results from reduced sphingolipid synthesis because of limiting amounts of palmitic acid (Bonaventure et al., 2003). The dwarf phenotype displayed by At *LCB1* RNAi plants supports this hypothesis. Interestingly, the *fatb* mutant, like At *LCB1* RNAi plants, did not have a detectable reduction in total amounts of sphingolipid long-chain bases when quantified on a per weight basis. The *Arabidopsis mosaic death1* (*mod1*) mutant, which carries a mutation in the gene for enoyl-acyl carrier protein reductase and has reduced de novo fatty acid synthesis, also displays a dwarf phenotype (Mou et al., 2000). It is possible that the smaller size of these plants is attributable primarily to reduced sphingolipid synthesis, as postulated for the *fatb* mutant, although the defect in *mod1* plants likely has a more global impact on metabolism.

The regulation of sphingolipid biosynthesis as well as the functions of these molecules in membrane ontogeny and in growth and development are still largely uncharacterized in plants. The functional identification of At LCB1 and the demonstration that SPT functions as a heteromeric enzyme in *Arabidopsis* lays the foundation for studies of the flux control that SPT asserts on the sphingolipid biosynthetic pathway in response to altered metabolism and environmental stimuli. In addition, the At *LCB1* RNAi plants will likely be useful tools for studies of sphingolipid-associated membrane trafficking in plant cells. Furthermore, as techniques for detailed analyses of sphingolipids in plants evolve, the At *LCB1* RNAi plants may help reveal the possible involvement of sphingolipid metabolites, including long-chain base phosphates, in the regulation of plant growth.

METHODS

Plant Material and Growth Conditions

For sterile growth, *Arabidopsis thaliana* (Col-0) seeds were surface-sterilized and sowed on Murashige and Skoog agar plates (Sigma-Aldrich) containing 3% sucrose. After 2 d of stratification at 4°C, the plates were maintained at 16 h of light/8 h of dark at 120 $\mu mol \cdot m^{-2} \cdot s^{-1}$ at 23°C. Soil-grown plants were maintained at 22°C and 50% humidity under either long-day conditions with a 16-h light (100 $\mu mol \cdot m^{-2} \cdot s^{-1}$)/8-h dark cycle or short-day conditions with an 8-h light (200 $\mu mol \cdot m^{-2} \cdot s^{-1}$)/16-h dark cycle. Unless indicated, plants were grown under a long-day regime.

Plasmid Construction for Plant Transformation

All PCR amplifications were conducted with *Pfu*-Ultra polymerase (Stratagene), and products were verified by sequencing. An At *LCB1* promoter–GUS reporter construct was generated by amplification of an ~2.0-kb sequence upstream of the start codon of At *LCB1* (At4g36480) using the sense and antisense oligonucleotides P29 and P30 (see Supplemental Table 1 online for the sequences of oligonucleotides.) The product was digested with *Hin*dIII and *Xba*I and cloned into the corresponding sites of binary vector pBI121 (Clontech) to generate a transcriptional fusion with the GUS coding region. The resulting plasmid was designated Pro_{LCB1}:GUS.

For genomic complementation of SALK_077745, an ~5-kb fragment of At *LCB1* was amplified from *Arabidopsis* (Col-0) genomic DNA by a pair of

primers, P3 and P4, as shown in Figure 5A. The amplified product was then digested with *Asc*I and *Pac*I and cloned into the binary vector pMDC123 (Curtis and Grossniklaus, 2003) in place of the cloning cassette to produce pMDC123_LCB1g. The ER marker construct, CSP-CFP-HDEL, was made by PCR amplification with oligonucleotides P7 and P8 using the cerulean variant form of CFP (provided by David Piston) as a template. The resulting PCR product, containing the signal peptide of basic chitinase (At3g12500) (Haseloff et al., 1997) and the ER retention signal (HDEL), was subcloned into vector pMDC32 using the *Asc*I and *Pac*I sites (Curtis and Grossniklaus, 2003).

For construction of pMDC32LCB1-EYFP, the EYFP gene was amplified by PCR with primers P9 and P10 using the plant expression vector pCAMBIA (CAMBIA) as a template. The product was introduced in place of the Gateway cassette in the plasmid PMDC32 to generate pMDC32YFP. The At *LCB1* cDNA was then amplified using primers P11 and P12, and the product was cloned into the *Asc*I and *Nco*I sites of pMDC32YFP to generate pMDC32LCB1-YFP.

An At *LCB1* RNAi suppression construct was generated using the pHellsgate8 RNAi Gateway vector system (Helliwell and Waterhouse, 2003). A 319-bp fragment of At *LCB1* was amplified using oligonucleotides P13 and P14, and the product was recombined with the donor vector pDOR221 (Invitrogen) to yield pENT_LCBIi. This plasmid was then reacted with the destination vector pHellsgate8 in an *att*L × *att*R recombination reaction according to the manufacturer's protocol (Invitrogen) to generate the final RNAi plasmid, pH8LCB1i. Another At *LCB1* RNAi construct was generated with the pHannibal vector (Helliwell and Waterhouse, 2003). The segment of the At *LCB1* open reading frame described above was amplified by PCR with two pairs of oligonucleotides, P15/P16 and P17/P18, and the products of the two reactions were cloned sequentially into the pHannibal vector. The resulting hairpin construct together with the cauliflower mosaic virus 35S promoter and the *ocs* terminator were released and inserted into the *Not*I site of binary vector pART27 to generate pHanLCB1i.

Arabidopsis Transformation and Selection

Binary vectors were introduced into *Agrobacterium tumefaciens* C58 by electroporation. Transgenic plants were generated by floral dip (Clough and Bent, 1998) of *Arabidopsis* (Col-0) (pH8LCB1i, Pro_{LCB1}:GUS) or heterozygous SALK_077745 (pMDC123_LCB1g) T-DNA and screened on Murashige and Skoog plates containing either 50 mg/L kanamycin monosulfate (pH8LCB1i, Pro_{LCB1}:GUS) or 10 mg/L glufosinate ammonium (pMDC123_LCB1g).

Saccharomyces cerevisiae Strains, Media, and Growth Conditions

Saccharomyces cerevisiae cells were grown according to standard procedures (Sherman et al., 1986). The *lcb1ΔKAN* knockout was generated by dissecting the heterozygous *lcb1Δ* knockout in the BY4743 background (Open Biosystems) on medium containing 15 μM phytosphingosine. The *lcb2Δ* knockout was generated by transforming a *LEU2*$^+$ disrupting fragment (Zhao et al., 1994) into a wild-type haploid strain (DHY4a, *MAT α, ura3-52, leu2 his3 lys2 met15*) derived from the dissection of the BY4743 diploid. The *lcb1ΔKAN lcb2ΔLEU* double mutant was obtained from tetrad dissection of a diploid generated by crossing the *lcb1ΔKAN* haploid with the *lcb2ΔLEU* haploid. The *lcb1ΔKAN tsc3ΔNAT* strain was constructed by disrupting *TSC3* in the *lcb1Δ* mutant strain using the *tsc3ΔNAT* disrupting allele that was constructed by replacing the coding sequence of *TSC3* with a NAT cassette based on the strategy described by Gable et al. (2000). Briefly, a *Kpn*I/*Xho*I-ended fragment containing the upstream flanking sequence of *TSC3* from 200 bp before the start codon to 30 bp past the start codon and an *Xho*I/*Eco*RI-ended fragment containing the downstream flanking sequence from 40 bp before the stop codon to 300 bp past the stop codon were generated by PCR. These fragments were ligated together and inserted between the *Kpn*I and *Eco*RI sites of pUC19, yielding a plasmid having an *Xho*I site replacing most of the *TSC3* coding sequence. An *Xho*I-end fragment containing the NAT gene (nourseothricin-resistance marker *NATMX*) was generated by PCR using primers P19 and P20 and the template, p4339, containing *NATMX4* DNA (Goldstein and McCusker, 1999; Tong et al., 2001). The *Xho*I-ended *NATR* fragment was ligated into the *Xho*I site, and the *tsc3ΔNAT* disrupting allele was liberated by digestion with *Kpn*I and *Eco*RI. The *lcb1Δ*, *lcb2Δ*, *lcb1Δ lcb2Δ*, and *lcb1Δ tsc3Δ* mutant strains were grown in YPD or SD medium containing 15 μM phytosphingosine and 0.2% Tergitol Nonidet P-40 (Sigma-Aldrich). To induce the expression of the At *LCB* genes under the control of the *GAL1* or *GAL10* promoter of the pESC vector, 2% galactose and 1% raffinose were added to the medium.

S. cerevisiae Expression Constructs

Expression of At *LCB1* and At *LCB2* was conducted using the yeast expression vector pESC-URA (Stratagene). The open reading frame of an At *LCB1* cDNA was amplified using oligonucleotides P21 and P22. The product was digested with *Bam*HI and *Xho*I and then cloned into the corresponding sites of pESC-URA, downstream of the *GAL1* promoter, to generate the plasmid pESC-URALCB1.

Similarly, the open reading frame of a cDNA for At *LCB2* (At5g23670) (Tamura et al., 2001) was amplified with oligonucleotides P23 and P24, digested with *Eco*RI and *Pac*I, and then cloned into the corresponding sites of pESC-URA, downstream of the *GAL10* promoter, to generate the plasmid pESC-URALCB2. Alternatively, the product was digested with *Eco*RI and *Pac*I and then cloned into the second multiple cloning site of pESC-URALCB1, downstream of the *GAL10* promoter, to generate pESC-URALCB1/LCB2.

Microsome Preparation

For preparation of microsomes from yeast, cells were pelleted and resuspended in MEM buffer (20 mM Tris-HCl, pH 7.5, containing 1 mM EGTA, 1 mM β-mercaptoethanol, 1 mM phenylmethylsulfonyl fluoride, 1 mM leupeptin, 1 mM aprotinin, and 1 mM pepstatin A). The cells were disrupted by bead beating, and cell debris was removed by centrifugation at 8000*g* for 10 min as described (Gable et al., 2000). Microsomes were recovered from the supernatant by centrifugation at 100,000*g* for 30 min. The microsomal pellet was washed once with MEM buffer, resuspended at 1 mL/g wet cell weight (~10 mg/mL protein) in the same buffer containing 33% glycerol, and stored at −80°C.

The protocol described by Lynch and Fairfield (1993) was used for isolation of microsomes from *Arabidopsis* with minor modifications. Approximately 20 g of leaves from 6-week-old *Arabidopsis* plants grown under short-day conditions was harvested and homogenized in 40 mL of cold homogenizing medium supplemented with a protease inhibitor cocktail (P9599; Sigma-Aldrich).

SPT Assay

SPT was assayed using yeast microsomal protein as described previously (Han et al., 2002) except that 0.2 mg of microsomal protein and 0.06 mM palmitoyl-CoA were used. Background incorporation of L-[γ-^{3}H]Ser was measured without the addition of palmitoyl-CoA and subtracted. Each assay was conducted in triplicate, and the average SPT activity was reported. The same protocol was used to assay SPT activity in plant microsomes.

Protein Gel Blotting

Before electrophoresis, proteins were heated at 70°C for 10 min in NuPAGE sample buffer (Invitrogen). Proteins were resolved using a 4 to 12% BisTris NuPAGE gel system (Invitrogen) according to the manufacturer's

instructions and transferred to nitrocellulose. The polyclonal antibodies to yeast LCB1 and LCB2 have been described previously (Gable et al., 2000). The anti-At LCB2 antibodies were generated from a washed inclusion body from *Escherichia coli* expression of the C-terminal 166 amino acids of At LCB2. Of note, although anti-yeast LCB1 and anti-At LCB2 antibodies were able to detect At LCB1 and At LCB2, respectively, in yeast microsomes after *GAL*-mediated expression, they were not suitable for detection of the native At LCB1 and At LCB2 in crude or microsomal extracts from *Arabidopsis* leaves. The blots were incubated with the primary antibodies (anti-yeast LCB1, 1:2500; anti-yeast LCB2, 1:2000; anti-At LCB2, 1:5000), washed, and then incubated with goat anti-rabbit horseradish peroxidase–conjugated antibody (Bio-Rad). They were developed using chemiluminescence detection reagents (ECL-Plus protein gel blotting detection systems; Amersham Biosciences).

RT-PCR and Quantitative RT-PCR

Total RNA was isolated from selected organs of 6-week-old wild-type (Col-0) *Arabidopsis* plants using the RNeasy plant kit (Qiagen) according to the manufacturer's protocol. Total RNA (1 μg) was first treated with DNase (Roche), and first-strand cDNA was subsequently synthesized using SuperScript III reverse transcriptase (Invitrogen) and oligo(dT) primer, according to manufacturer's instructions. A 2-μL aliquot of first-strand cDNA was used as template to amplify At *LCB1* or the gene for the ubiquitin-conjugating enzyme (At5g25760) in a 20-μL reaction. PCR amplification (33 cycles) was conducted with Taq DNA polymerase (New England Biolabs). The primers used for the amplification of At *LCB1*–derived cDNA were P25 and P26. The gene for the ubiquitin-conjugating enzyme (*UBC*; At5g25670) was used as an internal control (Czechowski et al., 2005). The primers used for the amplification of *UBC*-derived cDNA were P27 and P28.

Quantitative real-time PCR was conducted with total RNA that was isolated from leaves of 4-week-old T2 seedlings of At LCB1 RNAi and wild-type (Col-0) plants as described above. A 100-ng aliquot of each RNA sample after DNase treatment was amplified by PCR using the SuperScript III Platinum two-step qRT-PCR kit with SYBR Green (Invitrogen), according to the manufacturer's protocols. An Opticon 2 continuous fluorescence detector (Bio-Rad) interfaced with a thermocycler was used for the quantification of products. For each sample, PCR was conducted with At *LCB1*–specific primers (P25 and P26), and a parallel reaction was conducted using primers for the *UBC* control (P27 and P28). The efficiency of primer pairs was measured by calculating the slope of the log of cDNA dilutions versus ΔC_T ($C_{T,At\ LCB1} - C_{T,UBC}$), as described by Livak and Schmittgen (2001), and was demonstrated to be very close, which validated the use of the $2^{-\Delta\Delta C}$T method to calculate gene expression levels.

Detection of GUS Activity

Homozygous lines containing the construct Pro_{LCB1}:GUS were isolated from the T3 generation. Histochemical assays for GUS activity were performed according to the protocol described by Gallagher. (1992).

Characterization of T-DNA Insertion Mutants

Individual plants from a mixed population of SALK_077745 (T4 seeds; ABRC) were screened by PCR. The T-DNA disruption allele was verified using the oligonucleotides LBa1 (5′-TGGTTCACGTAGTGGGCCATCG-3′) and P2. The wild-type allele was amplified using P2 in combination with oligonucleotide P1 (Figure 5A). The insertion site was confirmed by sequencing the PCR product. Because no homozygous SALK_077745 T-DNA line could be verified, plants were propagated as heterozygotes.

Subcellular Localization and Microscopy

For subcellular localization studies of At LCB1, tobacco (*Nicotiana benthamiana*) leaves were coinfiltrated with *Agrobacterium* GV3101 harboring the plasmid At LCB1-EYFP or CSP-CFP-HDEL using previously described methods (English et al., 1997) with modifications. In short, *Agrobacterium* cultures at the log growth stage ($OD_{600} = 1.0$) were collected by centrifugation and resuspended in buffer containing 10 mM MES, pH 5.7, and 10 mM $MgCl_2$ to OD = 1.0 at 600 nm. Acetosyrigone was then added to the *Agrobacterium* solution at 100 μM. The resuspended cells were incubated at room temperature for 3 to 4 h before infiltration. The leaves were observed at 36 to 72 h after infiltration. CFP and EYFP fluorescence were observed using a confocal laser scanning microscope (Carl Zeiss LSM 510). The filter sets for CFP were excitation 458 nm and emission 480 to 520 nm, and those for EYFP were excitation 514 nm and emission 535 to 590 nm. Images were processed with an LSM 510 browser and Photoshop 6.0.

For observation of dissected seeds and GUS-stained tissues, a Nikon SMZ1500 dissection microscope attached to a digital camera (Retiga 1300; Qimaging) was used, and images were processed with IPLab software. Embryos, leaf epidermal cells, and seeds were cleared with Hoyer's solution and observed with a Nikon Eclipse E800 microscope equipped with a differential interference contrast apparatus (Nomarski optics) as described by Meinke (1994), and images were recorded with Openlab software (Improvision). For the measurement of mesophyll cells of petioles, tissues were peeled from the petiole of the fifth rosette leaf of wild-type or At *LCB1* RNAi plants and quickly stained with 0.4% (w/v) trypan blue (Sigma-Aldrich). Mesophyll cells were photographed, and the cell length was measured with Openlab software.

Analysis of Sphingolipid Long-Chain Bases

The total content and composition of sphingolipid long-chain bases were determined after strong alkaline hydrolysis of complex sphingolipids using a method based on that described by Morrison and Hay (1970). Lyophilized leaves (~10 mg) were thoroughly ground in 1 mL of 1,4-dioxane (Sigma-Aldrich) using a Potter-Elvehjem glass homogenizer. D-Erythro-C16-sphingosine (Matreya) was added to the homogenate as an internal standard, and the homogenate was transferred to a screw-cap test tube (13 × 100 mm). One milliliter of freshly prepared 10% (w/v) $BaOH_2 \cdot 8H_2O$ (Sigma-Aldrich) was then added to each sample. After mixing and evacuation of tubes with N_2, samples were heated at 110°C for 16 h. The samples were then cooled and extracted with the addition of 3 mL of chloroform and 1 mL of water. Upon mixing and centrifugation at 1000*g* for 5 min, the organic phase (containing free long-chain bases) was recovered and dried under N_2. *o*-Phthaldehyde derivatives of free long-chain bases were then prepared as described by Wright et al. (2003). *o*-Phthaldehyde derivatives of long-chain bases were analyzed with an Agilent 1100 HPLC apparatus outfitted with a ZORBAX Eclipse XDB-C18 reverse-phase column (4.6 mm × 250 mm; Agilent). Sample components were resolved with a gradient solvent system consisting of 80% methanol (solvent A) and 20% 5 mM potassium phosphate, pH 7.0 (solvent B) (7-min hold), to 90% solvent A and 10% solvent B over an 8-min linear gradient, and then, after a 10-min hold, to 100% solvent A over a 5-min linear gradient (1-min hold). The flow rate was 1.5 mL/min. *o*-Phthaldehyde–derivatized long-chain bases were detected by fluorescence with excitation at 340 nm and emission at 455 nm. Long-chain bases were quantified relative to the internal standard. The identities of long-chain bases were established by mobility relative to standards and by liquid chromatography–mass spectrometry structural analysis.

Analysis of the Long-Chain Base Composition of Sphingolipid Classes

Sphingolipids were extracted from 1 g of leaves harvested from wild-type and At *LCB1* RNAi suppression plants and partitioned into charged and neutral sphingolipid–enriched fractions using the protocol described by Markham et al. (2006). Monoglucosylceramides were purified from the

neutral sphingolipid–enriched fraction by silica solid-phase extraction followed by thin layer chromatography using procedures described by Cahoon and Lynch (1991) and Bonaventure et al. (2003).

The solvent-extracted plant residue, monoglucosylceramides, and aliquots from the total lipid extract and charged sphingolipid–enriched fractions were analyzed for long-chain base composition as described above.

DNA Gel Blot Analysis

DNA was isolated from *Arabidopsis* plants using the plant DNAzol reagent (Invitrogen). Approximately 8 μg of genomic DNA was digested with different combinations of restriction enzymes. DNA samples were electrophoresed at 30 V for 15 h and then transferred to Hybond N^+ nylon membranes (Amersham Bioscience). A 700-bp fragment of the neomycin phosphotransferase II gene was amplified by primers P31 and P32. The PCR product was then used to prepare a digoxigenin-labeled probe using the PCR DIG Probe Synthesis Kit (Roche). Hybridization and detection were conducted according to the protocol for the DIG High Primer DNA Labeling and Detection Starter Kit II (Roche). In short, hybridization was conducted with DIG Easy Hyb buffer (Roche) at 42°C overnight. After posthybridization washing, the blot was incubated sequentially in the blocking reagent and the antibody solution (antidigoxigenin alkaline phosphatase [1:10,000] diluted in blocking solution). After washing, the blot was incubated with the manufacturer-supplied development substrate at 37°C for 15 min before exposure to x-ray film for 0.5 to 1 h.

Phylogenetic Analysis

Amino acid sequences were aligned with ClustalW (Thompson et al., 1994) using Gonnet protein weight matrix (gap open penalty = 10, gap extension penalty = 0.2, gap separation distance = 4). Sequence alignments are provided in Supplemental Figure 3 online. Phylogenetic analysis of the aligned full-length sequences was conducted with MEGA 3.1 (Kumar et al., 2004) using neighbor joining (Saitou and Nei, 1987) and the p-distance model. Pairwise deletion was used for handling of sequence gaps, and 5000 bootstrap replicates were performed.

Accession Numbers

GenBank accession numbers for the amino acid sequences used in the phylogenetic analyses are as follows: At LCB1, NP_568005; At LCB2, NM_122272; Bc AONS, NP_977013; Ca LCB1, EAK97279; Ca LCB2, EAL03464; Cg LCB1, O54695; Cg LCB2, O54694; Hs LCB1, NP_006406; Hs LCB2, NP_004854; Kl LCB1, XP_451435; Kl LCB2, AAC49535; Mm LCB1, O35704; Mm LCB2, NP_035609; Os LCB1a, NP_920251; Os LCB1b, XP_468301; Os LCB2a, BAD88168; Os LCB2b, NP_914891; Sc LCB1, AAA34739; Sc LCB2, NP_010347; Sp sSPT, BAB56013; St LCB2, CAB44316; Td AONS, NP_972795; and Zm sSPT, YP_163005.

Supplemental Data

The following materials are available in the online version of this article.

Supplemental Table 1. Primer Sequences Used in Cloning, RT-PCR, T-DNA Mutant Characterization, and Synthesis of Probes for DNA Gel Blot Analyses.

Supplemental Figure 1. Microarray Data for the Expression of At *LCB1* in Different Organs of *Arabidopsis*.

Supplemental Figure 2. DNA Gel Blot Analysis of the T-DNA Insertion in Genomic DNA from SALK-077745 (At *lcb1-1*).

Supplemental Figure 3. Amino Acid Sequence Alignments of Selected LCB1, LCB2, AONS, and Soluble SPT Polypeptides.

ACKNOWLEDGMENTS

We thank Jan Jaworski, Jonathan Markham, and Daniel Lynch for helpful discussions and Yan Fu for assistance with phylogenetic analyses. We also thank Jia Li for technical assistance, Howard R. Berg for assistance with differential interference contrast microscopy, Robert Mullen for helpful comments on ER localization studies, and Rebecca Cahoon for critical reading of the manuscript. We acknowledge the ABRC (Ohio State University) for providing the SALK T-DNA mutant lines for At *LCB1*. This work was supported by National Science Foundation Arabidopsis 2010 Grants MCB-0313466 to T.M.D. and MCB-0312559 to E.B.C.

Received December 31, 2005; revised October 24, 2006; accepted November 10, 2006; published December 28, 2006.

REFERENCES

Adachi-Yamada, T., Gotoh, T., Sugimura, I., Tateno, M., Nishida, Y., Onuki, T., and Date, H. (1999). De novo synthesis of sphingolipids is required for cell survival by down-regulating c-Jun N-terminal kinase in *Drosophila* imaginal discs. Mol. Cell. Biol. **19,** 7276–7286.

Alexeev, D., Alexeeva, M., Baxter, R.L., Campopiano, D.J., Webster, S.P., and Sawyer, L. (1998). The crystal structure of 8-amino-7-oxononanoate synthase: A bacterial PLP-dependent, acyl-CoA-condensing enzyme. J. Mol. Biol. **284,** 401–419.

Alonso, J.M., et al. (2003). Genome-wide insertional mutagenesis of *Arabidopsis thaliana*. Science **301,** 653–657.

Asai, T., Stone, J.M., Heard, J.E., Kovtun, Y., Yorgey, P., Sheen, J., and Ausubel, F.M. (2000). Fumonisin B1-induced cell death in Arabidopsis protoplasts requires jasmonate-, ethylene-, and salicylate-dependent signaling pathways. Plant Cell **12,** 1823–1836.

Astner, I., Schulze, J.O., van den Heuvel, J., Jahn, D., Schubert, W.D., and Heinz, D.W. (2005). Crystal structure of 5-aminolevulinate synthase, the first enzyme of heme biosynthesis, and its link to XLSA in humans. EMBO J. **24,** 3166–3177.

Bonaventure, G., Salas, J.J., Pollard, M.R., and Ohlrogge, J.B. (2003). Disruption of the *FATB* gene in Arabidopsis demonstrates an essential role of saturated fatty acids in plant growth. Plant Cell **15,** 1020–1033.

Bonhomme, S., Horlow, C., Vezon, D., de Laissardière, S., Guyon, A., Férault, M., Marchand, M., Bechtold, N., and Pelletier, G. (1998). T-DNA mediated disruption of essential gametophytic genes in *Arabidopsis* is unexpectedly rare and cannot be inferred from segregation distortion alone. Mol. Gen. Genet. **260,** 444–452.

Borner, G.H., Sherrier, D.J., Weimar, T., Michaelson, L.V., Hawkins, N.D., Macaskill, A., Napier, J.A., Beale, M.H., Lilley, K.S., and Dupree, P. (2005). Analysis of detergent-resistant membranes in Arabidopsis. Evidence for plasma membrane lipid rafts. Plant Physiol. **137,** 104–116.

Buede, R., Rinker-Schaffer, C., Pinto, W.J., Lester, R.L., and Dickson, R.C. (1991). Cloning and characterization of *LCB1*, a *Saccharomyces* gene required for biosynthesis of the long-chain base component of sphingolipids. J. Bacteriol. **173,** 4325–4332.

Cahoon, E.B., and Lynch, D.V. (1991). Analysis of glucocerebrosides of rye (*Secale cereale* L. cv Puma) leaf and plasma membrane. Plant Physiol. **95,** 58–68.

Carter, H.E., Hendry, R.A., Nojima, S., Stanacev, N.Z., and Ohno, K. (1961). Biochemistry of the sphingolipids. XIII. Determination of the structure of cerebrosides from wheat flour. J. Biol. Chem. **236,** 743–746.

Clough, S.J., and Bent, A.F. (1998). Floral dip: A simplified method for *Agrobacterium*-mediated transformation of *Arabidopsis thaliana*. Plant J. **16,** 735–743.

Coursol, S., Fan, L.M., Le Stunff, H., Spiegel, S., Gilroy, S., and Assman, S.M. (2003). Sphingolipid signaling in *Arabidopsis* guard cells involves heterotrimeric G proteins. Nature **423,** 651–654.

Coursol, S., Le Stunff, H., Lynch, D.V., Gilroy, S., Assmann, S.M., and Spiegel, S. (2005). Arabidopsis sphingosine kinase and the effects of phytosphingosine-1-phosphate on stomatal aperture. Plant Physiol. **137,** 724–737.

Curtis, M.D., and Grossniklaus, U. (2003). A gateway cloning vector set for high-throughput functional analysis of genes in *planta*. Plant Physiol. **133,** 462–469.

Czechowski, T., Stitt, M., Altmann, T., Udvardi, M.K., and Scheible, W.R. (2005). Genome-wide identification and testing of superior reference genes for transcript normalization in Arabidopsis. Plant Physiol. **139,** 5–17.

Dickson, R.C. (1998). Sphingolipid functions in *Saccharomyces cerevisiae*: Comparison to mammals. Annu. Rev. Biochem. **67,** 27–48.

English, J.J., Davenport, G.F., Elmayan, T., Vaucheret, H., and Baulcombe, D.C. (1997). Requirement of sense transcription for homology-dependent virus resistance and trans-inactivation. Plant J. **12,** 597–603.

Gable, K., Han, G., Monaghan, E., Bacikova, D., Natarajan, M., Williams, R., and Dunn, T.M. (2002). Mutations in the yeast *LCB1* and *LCB2* genes, including those corresponding to the hereditary sensory neuropathy type I mutations, dominantly inactivate serine palmitoyltransferase. J. Biol. Chem. **277,** 10194–10200.

Gable, K., Slife, H., Bacikova, D., Monaghan, E., and Dunn, T.M. (2000). Tsc3p is an 80-amino acid protein associated with serine palmitoyltransferase and required for optimal enzyme activity. J. Biol. Chem. **275,** 7597–7603.

Gallagher, S.R., ed (1992). GUS Protocols: Using the GUS Gene as a Reporter of Gene Expression. (San Diego, CA: Academic Press).

Gechev, T.S., Gadjev, I.Z., and Hille, J. (2004). An extensive microarray analysis of AAL-toxin-induced cell death in *Arabidopsis thaliana* brings new insights into the complexity of programmed cell death in plants. Cell. Mol. Life Sci. **61,** 1185–1197.

Goldstein, A.L., and McCusker, J.H. (1999). Three new dominant drug resistance cassettes for gene disruption in *Saccharomyces cerevisiae*. Yeast **15,** 1541–1553.

Gong, J., Kay, C.J., Barber, M.J., and Ferreira, G.C. (1996). Mutations at a glycine loop in aminolevulinate synthase affect pyridoxal phosphate cofactor binding and catalysis. Biochemistry **35,** 14109–14117.

Han, G., Gable, K., Kohlwein, S.D., Beaudoin, F., Napier, J.A., and Dunn, T.M. (2002). The *Saccharomyces cerevisiae* YBR159w gene encodes the 3-ketoreductase of the microsomal fatty acid elongase. J. Biol. Chem. **277,** 35440–35449.

Hanada, K. (2003). Serine palmitoyltransferase, a key enzyme of sphingolipids metabolism. Biochim. Biophys. Acta **1632,** 16–30.

Hanada, K., Hara, T., and Nishijima, M. (2000). Purification of the serine palmitoyltransferase complex responsible for sphingoid base synthesis by using affinity peptide chromatography techniques. J. Biol. Chem. **275,** 8409–8415.

Hanada, K., and Nishijima, M. (2003). Purification of mammalian serine palmitoyltransferase, a hetero-subunit enzyme for sphingolipid biosynthesis, by affinity-peptide chromatography. Methods Mol. Biol. **228,** 163–174.

Hanada, K., Nishijima, M., Kiso, M., Hasegawa, A., Fujita, S., Ogawa, T., and Akamatsu, Y. (1992). Sphingolipids are essential for the growth of Chinese hamster ovary cells. Restoration of the growth of a mutant defective in sphingoid base biosynthesis by exogenous sphingolipids. J. Biol. Chem. **267,** 23527–23533.

Haseloff, J., Siemering, K.R., Prasher, D.C., and Hodge, S. (1997). Removal of a cryptic intron and subcellular localization of green fluorescent protein are required to mark transgenic Arabidopsis plants brightly. Proc. Natl. Acad. Sci. USA **94,** 2122–2127.

Helliwell, C., and Waterhouse, P. (2003). Constructs and methods for high-throughput gene silencing in plants. Methods **30,** 289–295.

Hojjati, M.R., Li, Z., and Jiang, X.C. (2005). Serine palmitoyl-CoA transferase (SPT) deficiency and sphingolipid levels in mice. Biochim. Biophys. Acta **1737,** 44–51.

Ikushiro, H., Hayashi, H., and Kagamiyama, H. (2001). A water-soluble homodimeric serine palmitoyltransferase from *Sphingomonas paucimobilis* EY2395T strain. Purification, characterization, cloning, and overproduction. J. Biol. Chem. **276,** 18249–18256.

Imai, H., and Nishiura, H. (2005). Phosphorylation of sphingoid long-chain bases in Arabidopsis: Functional characterization and expression of the first sphingoid long-chain base kinase gene in plants. Plant Cell Physiol. **46,** 375–380.

Kaul, K., and Lester, R.L. (1978). Isolation of six novel phophoinositol-containing sphingolipids from tobacco leaves. Biochemistry **17,** 3569–3575.

Kumar, S., Tamura, K., and Nei, M. (2004). MEGA3: Integrated software for molecular evolutionary genetics analysis and sequence alignment. Brief. Bioinform. **5,** 150–163.

Liang, H., Yao, N., Song, J.T., Luo, S., Lu, H., and Greenberg, J.T. (2003). Ceramide phosphorylation modulates programmed cell death in plants. Genes Dev. **17,** 2636–2641.

Livak, K.J., and Schmittgen, T. (2001). Analysis of relative gene expression data using real-time quantitative PCR and the $2^{-\Delta\Delta CT}$ method. Methods **25,** 402–408.

Lynch, D.V., and Dunn, T.M. (2003). An introduction to plant sphingolipids and a review of recent advances in understanding their metabolism and function. New Phytol. **161,** 677–702.

Lynch, D.V., and Fairfield, S.R. (1993). Sphingolipid long-chain base synthesis in plants. Characterization of serine palmitoyltransferase activity in squash fruit microsomes. Plant Physiol. **103,** 1421–1429.

Lynch, D.V., and Steponkus, P.L. (1987). Plasma membrane lipid alterations associated with cold acclimation of winter rye seedlings (*Secale cereale* L. cv Puma). Plant Physiol. **83,** 761–767.

Markham, J.E., Li, J., Cahoon, E.B., and Jaworski, J.G. (2006). Plant sphingolipids: Separation and identification of major sphingolipid classes from leaves. J. Biol. Chem. **281,** 22684–22694.

Meinke, D.W. (1994). Seed development in *Arabidopsis thaliana*. In Arabidopsis, E.M. Meyerowitz and C.R. Somerville, eds (Cold Spring Harbor, NY: Cold Spring Harbor Laboratory Press), pp. 253–295.

Mongrand, S., Morel, J., Laroche, J., Claverol, S., Carde, J.P., Hartmann, M.A., Bonneu, M., Simon-Plas, F., Lessire, R., and Bessoule, J.J. (2004). Lipid rafts in higher plant cells: Purification and characterization of Triton X-100-insoluble microdomains from tobacco plasma membrane. J. Biol. Chem. **279,** 36277–36286.

Morrison, W.R., and Hay, J.D. (1970). Polar lipids in bovine milk. II. Long-chain bases, normal and 2-hydroxy fatty acids, and isomeric cis and trans monoenoic fatty acids in the sphingolipids. Biochim. Biophys. Acta **202,** 460–467.

Mou, Z., He, Y., Dai, Y., Liu, X., and Li, J. (2000). Deficiency in fatty acid synthase leads to premature cell death and dramatic alterations in plant morphology. Plant Cell **12,** 405–418.

Nagiec, M.M., Baltisberger, J.A., Wells, G.B., Lester, R.L., and Dickson, R.C. (1994). The *LCB2* gene of *Saccharomyces* and the related *LCB1* gene encode subunits of serine palmitoyltransferase, the initial enzyme in sphingolipid synthesis. Proc. Natl. Acad. Sci. USA **91,** 7899–7902.

Nagiec, M.M., Lester, R.L., and Dickson, R.C. (1996). Sphingolipid synthesis: Identification and characterization of mammalian cDNAs encoding the Lcb2 subunit of serine palmitoyltransferase. Gene **177,** 237–241.

Ng, C.K., Carr, K., McAinsh, M.R., Powell, B., and Hetherington, A.M. (2001). Drought-induced guard cell signal transduction involves sphingosine-1-phosphate. Nature **410,** 596–599.

Saitou, N., and Nei, M. (1987). The neighbor-joining method: A new method for reconstructing phylogenetic trees. Mol. Biol. Evol. **4,** 406–425.

Schmid, M., Davison, T.S., Henz, S.R., Pape, U.J., Demar, M., Vingron, M., Schölkopf, B., Weigel, D., and Lohmann, J.U. (2005). A gene expression map of *Arabidopsis thaliana* development. Nat. Genet. **37,** 501–506.

Sherman, F., Fink, G.R., and Hicks, J.B. (1986). Methods in Yeast Genetics. (Cold Spring Harbor, NY: Cold Spring Harbor Laboratory).

Spassieva, S.D., Markham, J.E., and Hille, J. (2002). The plant disease resistance gene *Asc*-1 prevents disruption of sphingolipid metabolism during AAL-toxin-induced programmed cell death. Plant J. **32,** 561–572.

Sperling, P., Franke, S., Lüthje, S., and Heinz, E. (2005). Are glucocerebrosides the predominant sphingolipids in plant plasma membranes? Plant Physiol. Biochem. **43,** 1031–1038.

Sperling, P., and Heinz, E. (2003). Plant sphingolipids: Structural diversity, biosynthesis, first genes and functions. Biochim. Biophys. Acta **1632,** 1–15.

Spiegel, S., and Milstien, S. (2003). Sphingosine 1-phosphate: An enigmatic signalling lipid. Nat. Rev. Mol. Cell Biol. **4,** 397–407.

Tamura, K., Musuhashi, M., Hara-Nishimura, I., and Imai, H. (2001). Characterization of an Arabidopsis cDNA encoding a subunit of serine palmitoyltransferase, the initial enzyme in sphingolipid biosynthesis. Plant Cell Physiol. **42,** 1271–1281.

Thompson, J.D., Higgins, D.G., and Gibson, T.J. (1994). CLUSTAL W: Improving the sensitivity of progressive multiple sequence alignment through sequence weighting, position-specific gap penalties and weight matrix choice. Nucleic Acids Res. **22,** 4673–4680.

Tong, A.H., et al. (2001). Systematic genetic analysis with ordered arrays of yeast deletion mutants. Science **294,** 2364–2368.

Wang, H., Li, J., Bostock, R.M., and Gilchrist, D.G. (1996). Apoptosis: A functional paradigm for programmed plant cell death induced by a host-selective phytotoxin and invoked during development. Plant Cell **8,** 375–391.

Wright, B.S., Snow, J.W., O'Brien, T.C., and Lynch, D.V. (2003). Synthesis of 4-hydroxysphinganine and characterization of sphinganine hydroxylase activity in corn. Arch. Biochem. Biophys. **415,** 184–192.

Yasuda, S., Nishijima, M., and Hanada, K. (2003). Localization, topology, and function of the LCB1 subunit of serine palmitoyltransferase in mammalian cells. J. Biol. Chem. **278,** 4176–4183.

Yoshida, S., and Uemura, M. (1986). Lipid composition of plasma membranes and tonoplasts isolated from etiolated mung bean (*Vigna radiata* L.). Plant Physiol. **82,** 807–812.

Zhang, K., Showalter, M., Revollo, J., Hsu, F.F., Turk, J., and Beverley, S.M. (2003). Sphingolipids are essential for differentiation but not growth in *Leishmania*. EMBO J. **22,** 6016–6026.

Zhao, C., Beeler, T., and Dunn, T. (1994). Suppressors of the Ca(2+)-sensitive yeast mutant (csg2) identify genes involved in sphingolipid biosynthesis. Cloning and characterization of *SCS1*, a gene required for serine palmitoyltransferase activity. J. Biol. Chem. **269,** 21480–21488.

Zheng, H., Rowland, O., and Kunst, L. (2005). Disruptions of the Arabidopsis enoyl-CoA reductase gene reveal an essential role for very-long-chain fatty acid synthesis in cell expansion during plant morphogenesis. Plant Cell **17,** 1467–1481.

Zimmermann, P., Hirsch-Hoffmann, M., Hennig, L., and Gruissem, W. (2004). GENEVESTIGATOR. Arabidopsis microarray and analysis toolbox. Plant Physiol. **136,** 2621–2632.